EFFECT OF SIZE AND STRAIN RATE ON DEFORMATION BEHAVIOUR OF $Cu_{50}Zr_{50}$ METALLIC GLASS: A MOLECULAR DYNAMICS SIMULATION STUDY

A Thesis submitted in partial fulfilment of the requirements for the Degree

Of

Bachelor of Technology (B. Tech)

In

METALLURGICAL & MATERIALS ENGINEERING

By

SATYANARAYAN DHAL (108MM026)

YADLAPALLI RAJA (108MM031)

Department of Metallurgical & Materials Engineering
National Institute of Technology
Rourkela-769008
2012

EFFECT OF SIZE AND STRAIN RATE ON DEFORMATION BEHAVIOUR OF $Cu_{50}Zr_{50}$ METALLIC GLASS: A MOLECULAR DYNAMICS SIMULATION STUDY

A Thesis submitted in partial fulfilment of the requirements for the Degree

Of

Bachelor of Technology (B. Tech)

In

METALLURGICAL & MATERIALS ENGINEERING

By

SATYANARAYAN DHAL (108MM026)

YADLAPALLI RAJA (108MM031)

Under the Guidance of

Prof. N. YEDLA

Department of Metallurgical & Materials Engineering
National Institute of Technology
Rourkela-769008
2012

DEPARTMENT OF METALLURGICAL & MATERIALS ENGINEERING

NATIONAL INSTITUTE OF TECHNOLOGY

ROURKELA-769008, INDIA

CERTIFICATE

This is to certify that the project entitled "**Effect of size and strain rate on deformation behaviour of $Cu_{50}Zr_{50}$ metallic glass: A molecular dynamics simulation study**" submitted by **Mr. SATYANARAYAN DHAL (108MM026) and Mr. YADLAPALLI RAJA (108MM031)** in partial fulfilments for the requirements for the award of **Bachelor of Technology** Degree in **Metallurgical & Materials Engineering** at **National Institute of Technology, Rourkela** (Deemed University) is an authentic work carried out by them under my supervision and guidance.

To the best of my knowledge, the matter embodied in the report has not been submitted to any other University / Institute for the award of any Degree or Diploma.

Date: 10.05.2012

Prof. N. YEDLA

Department of Metallurgical & Materials Engineering

National Institute of Technology

Rourkela-769008

ACKNOWLEDGEMENT

We would like to thank **NIT Rourkela** for giving us the opportunity to use its resources and work in such a challenging environment. First and foremost, we take this opportunity to express our deep regards and sincere gratitude to our guide **Prof. N. Yedla** for his able guidance and constant encouragement during our project work. This project would not have been possible without his help and the valuable time that he has given us amidst his busy schedule.

We would also like to express our utmost gratitude to **Prof. B.C Ray, HOD, Metallurgical & Materials engineering** for allowing us to use the departmental facilities and for his valuable suggestions and encouragements at various stages of the work.

We would also like to extend our hearty gratitude to our friends and senior students of this department who have always encouraged and supported in doing our work. Last but not the least, we would like to thank all the staff members of Department of Metallurgical &Materials Engineering who have been very cooperative with us.

Place: NIT-Rourkela **Satyanarayan Dhal (108MM026)**

Date: 10.05.2012 **Yadlapalli Raja (108MM031)**

Metallurgical & Materials Engineering

ABSTRACT

Metallic glasses or amorphous metals have attracted considerable attention due to their unique properties and have been evolved as a potential field of research in recent years. The recent discovery of new glass-forming compositions makes it possible to produce metallic glasses in bulk shapes. Bulk metallic glasses provides a promising future to revolutionize the field of structural materials with combinations of strength, elastic limit, toughness, wear resistance and corrosion resistance. Some of their superior properties over crystalline metals have made them a versatile engineering material for many commercial applications now-a-days. Since the fabrication of metallic glasses require high cooling rates and sometimes practically impossible in laboratory conditions, so computational approaches are extensively used to explore various properties and behaviour of metallic glasses.

This project work presents a molecular dynamics simulation study on deformation behaviour of $Cu_{50}Zr_{50}$ metallic glass where the effect of parameters like sample-size and strain rate on the tensile deformation behaviour have been thoroughly studied. Computational methods to create alloy models, subsequent quenching and further tensile deformation have been mentioned. Stress-strain plots were drawn at same strain rate for different sizes of alloy models and at different strain rates for a particular size. Reasons for getting different stress-stress curves for different conditions have also been discussed.

CONTENTS

List of Figures:

List of tables:

Chapter-1

Introduction

1.1 Introduction to Metallic Glasses:

Today, the overwhelming development of science and technology has paved the way for scientists to find out new materials for high technology applications. The materials used for high tech applications are designed to have maximum performance at optimum conditions. Some of the modern engineering materials which have attracted considerable attention of material scientists are metallic glasses, shape memory alloys (SMA), nanophase materials, carbon nanotubes etc. Here the focus of this project work is on the metallic glasses.

In a lay man view, a glass is any material that can be cooled from a liquid to a solid without crystallization. Most metals do crystallize as they cool, arranging their atoms into a highly regular spatial pattern called a lattice. But if by any how crystallization can be stopped or does not occur, and the atoms settle into a nearly random arrangement, the final form is a metallic glass.

So metallic glass or glassy metal also known as amorphous metal is a solid metallic material, usually an alloy, with a disordered atomic arrangement. Most metals are crystalline in their solid state, which means they have a highly ordered arrangement of atoms. On the other hand, amorphous metals are non-crystalline, and thus are glasses. But unlike the usual glasses, such as window-glass, which are insulators, amorphous metals have good electrical conductivity. Fig. 1 shows bulk metallic glass samples produced by suction casting technique [1].

Fig. 1.1. Samples of bulk amorphous metal.

1.2 Evolution of Metallic Glasses:

The evolution of metallic glasses started with production of an alloy $Au_{75}Si_{25}$ at Caltech university by Jr W. Klement Willens and Duwez in 1960 [2]. To produce these glass-forming alloys, the cooling rate should be extremely high on the order of 10^6 K/s to avoid crystallization. In order to achieve such a high cooling rate, metallic glasses have to be produced in a limited number of forms typically ribbons, foils, or wires having one dimension so small that heat could be extracted quickly enough to achieve the necessary cooling rate. As a result, metallic glass specimens (with a few exceptions) were limited to thicknesses of less than one hundred micrometers.

In 1969, an alloy of 77.5% palladium, 6% copper, and 16.5% silicon was produced having critical cooling rate between 100 to 1000 K/s.

In 1976, a new technique to manufacture thin ribbons of amorphous metal on a supercooled fast-spinning wheel came into picture thanks to H. Liebermann and C. Graham [3]. This was an alloy of iron, nickel, phosphorus and boron.

The material known as *Metglas*, was commercialized in early 1980s and was used for low-loss power distribution transformers (Amorphous metal transformer).

In the early 1980s, glassy ingots with 5 mm diameter were produced from the alloy of 55% palladium, 22.5% lead, and 22.5% antimony, by surface etching followed with heating-cooling cycles. Using boron oxide flux, the achievable thickness was increased to a centimeter.

In 1988, alloys of lanthanum, aluminium, and copper ore were found to have highly glass-forming ability [1].

In the 1990s, with some effective research, new alloys of glass were developed at much lower cooling rates as low as one kelvin per second through casting into metallic molds. These were called as bulk metallic glasses. Alloys with the best glass-forming ability are based on zirconium and palladium [1].

Then many amorphous alloys were formed by based on a phenomenon called the "confusion" effect. Such alloys contain so many different elements (often four or more) that upon cooling at sufficiently high rates, the constituent atoms simply cannot arrange themselves into a ordered state before their mobility is stopped. In this way, the random disordered state of the atoms was "locked in" [1].

In 1992, the commercial amorphous alloy, Vitreloy (41.2% Zr, 13.8% Ti, 12.5% Cu, 10% Ni, and 22.5% Be), was developed at Caltech, as a part of Department of Energy and NASA research of new aerospace materials [1].

In 2004, two groups succeeded in producing bulk amorphous steel, one at Oak Ridge National Laboratory, and the other at University of Virginia. The Oak Ridge group refers to

their product as "glassy steel". The product is non-magnetic at room temperature and significantly stronger than conventional steel.

1.3 Glass formation and production techniques:

All metals prefer to form crystals as the metal atoms easily form structured bonds with other atoms. Even when the metal is melted, some of that arrangement carries over into the liquid. This makes the formation of a crystal the preferred pathway once the melt is cooled down again. Glass, on the other hand, is amorphous, which means that the atoms are disordered and there is no long-range periodicity. This is not something metals prefer. So metallic glass is a very different entity which needs very careful attention to produce.

There are several glass forming alloys which have been discovered in recent years. Some of them can be easily formed, some require very high cooling rates which is sometimes impossible to attain under laboratory conditions. So the ease with which a metallic glass can be produced is called glass forming ability. So many factors affect the glass forming ability. Those are [4]:

- The system should be multi-component so that the disordered state can be achieved easily.
- The enthalpy of glass formation should be negative for the glass formation to be thermodynamically favourable.
- The size difference between atoms of different components should be less.

Apart from these, researchers have proposed two criteria for glass formation. They are structural criterion and kinetic criterion. Structural criteria deals with geometrical atomic arrangement, bonding and atomic size effect and predict glass formation.

Many of the structural theories have been reviewed by Rawson and Cahn. The kinetic criterion developed mainly by Turnbull and Cohen (1960) and Turnbull (1969) [5] relates the rate of cooling to the kinetics of crystallization. Glass formation thus becomes a question of how fast a given liquid must be quenched in order that detectable crystallization can be prevented. The two criteria are complementary, since both the criteria implies that it is the particular structural characteristics that inhibits nucleation or growth of the crystalline phase.

An important feature of glass formation is the glass formation transition temperature denoted as Tg. Below are some important points about T_g:

- The glass transition temperature (T_g) of a non-crystalline material is the critical temperature at which the material changes its behavior from being 'glassy'(hard and brittle) to being 'rubbery'(elastic and flexible).
- At a temperature below T_g, large-scale molecular motion is not possible because the material is essentially frozen. If it is at a temperature above its T_g, molecular motion on the scale of its repeat unit (such as a single monomer in a polymer) takes place, allowing it to be 'soft' or 'rubbery'.
- T_g is affected by time, since it involves atomic or molecular motion i.e., the mechanical behavior of an amorphous material depends on how fast a load is applied to it. The faster a load is applied to a material at its T_g, the more glassy its behavior would be because its atoms or molecules are not given enough time to 'move.' Thus, even if an amorphous material is at its T_g, it can break in a 'glass-like' fashion if the loading rate applied to it is too high.

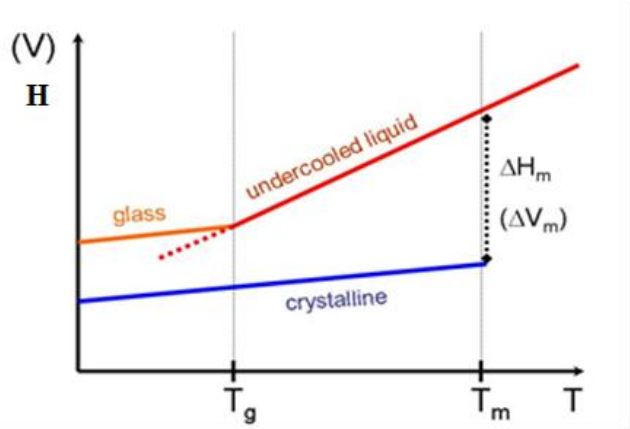

Fig. 1.2. Showing glass transition temperature, Tg.

Since high quenching rate is required to produce a metallic glass, some of the widely used rapid quenching techniques are [5]:

Liquid quenching:

In this method, a small liquid globule was propelled into small droplets by means of a Shock tube and the droplets were sprayed into thin foil on a copper substrate. Quenched samples produced were irregular in shape with varying thickness from about 1 pm to 10 pm.

Atomic condensation:

In this method a highly disordered structure is achieved by lowering the mobility of the atoms of a system so that the atoms condense without crystallization.vapour condensation at liquid helium temperature has yielded high superconducting amorphous films of Bi, Ga, As, Sb and Be.

Ion implantation:

Ion implantation has been gaining popularity as a method to introduce atoms into a surface and modify surface and bulk properties of many materials. Mechanisms of amorphization by ion implantation, however, remain unclear. When the concentration of ionic implants reaches a critical value, amorphous layers form.

1.4 Special properties of Metallic Glasses [1]:

- Viscosity is very high in molten state.This high viscosity prevents the atoms moving enough to form an ordered lattice.
- The glassy structure also results in low shrinkage during cooling and resistance to plastic deformation. The absence of grain boundaries, the weak spots of crystalline materials, leads to wear and corrosion resistance.
- Amorphous metals are also much tougher and less brittle than oxide glasses and ceramics.
- Thermal conductivity of amorphous materials is lower than that of crystalline metal. As formation of amorphous structure is based on fast cooling, this limits the maximum achievable thickness of amorphous structures.
- The alloys of boron, silicon, phosphorus, and other glass formers with magnetic metals like iron, cobalt, nickel have high magnetic susceptibility, with low coercivity and high electrical resistance.
- Usually the conductivity of a metallic glass is of the same low order of magnitude as of a molten metal just above the melting point. The high resistance leads to low losses

by eddy currents when subjected to alternating magnetic fields, a property useful for e.g. transformer magnetic cores.

- Amorphous alloys used to be stronger than crystalline alloys of similar chemical composition, and they can sustain larger reversible ("elastic") deformations than crystalline alloys. Amorphous metals derive their strength directly from their non-crystalline structure, which does not have any of the defects (such as dislocations) that limit the strength of crystalline alloys. One modern amorphous metal, known as Vitreloy, has a tensile strength that is almost twice that of high-grade titanium.
- Metallic glasses show poor ductility at room temperature and tend to fail suddenly when loaded in tension, which limits their low temperature applications.

1.5 Applications of Metallic Glasses [1]:

- They are used in nuclear reactors as they are least affected by magnetic radiation
- They behave as superconductors hence they are used in production of high magnetic field.
- They have high electrical resistance they are used to make computer memories.
- They provide very good corrosion resistance, so they can be used in surgical clips and marine vessels.
- Since they are malleable and ductile, they are used in filament windings.
- As they are very strong they are used to make different kinds of springs, Pressure sensors in various vehicles including automobiles.

- Bulk amorphous alloys called as true glasses e.g. they soften and flow upon heating can be easily which facilitates their commercial use in sports equipment, medical devices, and electronic equipment.

- Thin films of amorphous metals can be deposited via high velocity oxygen fuel technique as protective coatings.

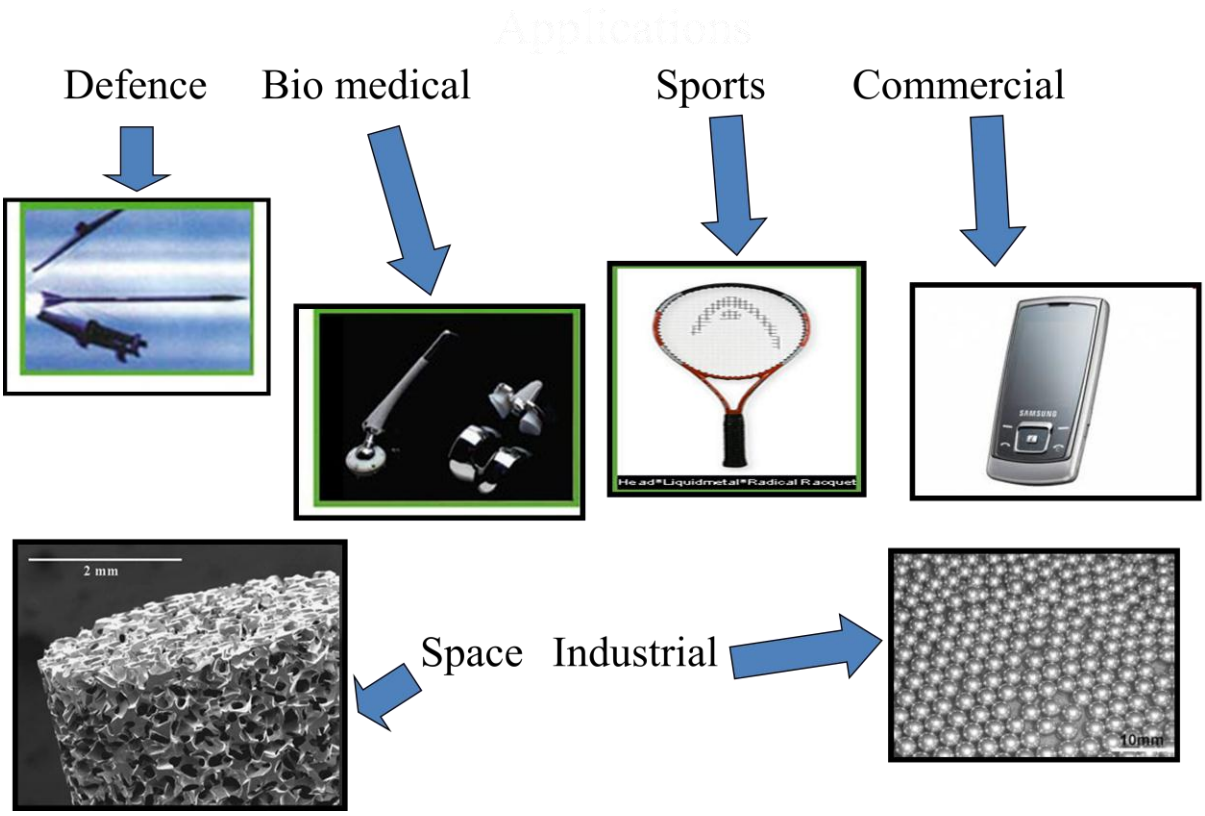

Fig. 1.3. Some potential applications of metallic glasses [1].

1.6 Deformation Mechanism in Metallic glasses:

It is well known that mechanical properties of crystalline materials are strongly dependent on the crystal structure and the plastic deformation is mediated by dislocations, whereas in glass due to the disordered atomic structure the deformation mechanism is different to that of crystalline materials. In spite of lacking long range- order metallic glasses possess short range ordering as proposed from several atomic packing model studies Regardless of the atomic packing the total volume of the glass can be separated into space occupied by the atomic clusters and the empty space between the clusters. The empty space is termed as free volume and around it constitutes atoms that have lower atomic coordination than those in densely packed atomic clusters. Further, the bonds are metallic in character; and hence amorphous alloys can be readily strained resulting in changes in atomic level through changes in neighborhood i.e. atomic bonds can be broken and reformed. However, an amorphous metal due to the lack of long-range ordering the exact nature of local atomic motion during deformation is not fully resolved. In spite of the above, there is a general consensus that deformation occurs by local rearrangement of atoms that can accommodate shear strain. Two theoretical models; based on free-volume model [6] and the other on shear transformation [7]. Have been proposed for explaining the deformation mechanisms in glass which are briefly described below:

(a) Free volume model:

Metallic glass packing models suggested that the atomic structure comprises of atomic clusters plus the empty space between them. The empty space between these clusters is termed as ‘free volume’ in which atomic rearrangements occur without effecting the surroundings significantly by application of temperature or stress and these are the preferred

regions for destabilization of the glassy structure. Spaepen [6], proposed the modes of deformation (inhomogeneous and homogeneous) in metallic glasses where homogeneous deformation occurs at low stresses and high temperature while that inhomogeneous deformation occurs by local softening at high stresses and low temperatures. He stated that at high levels of stress; free volume can be created by squeezing the atom into neighboring hole as shown in Fig. 1.4a, competing this process is the annihilation of free volume by series of diffusional jumps (Fig. 1.4b).

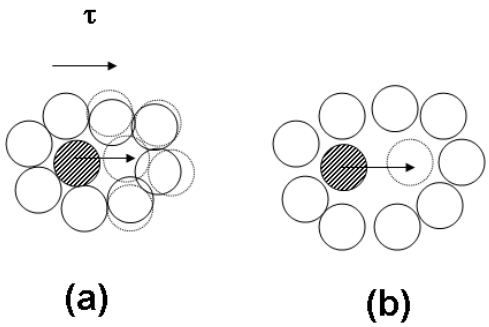

Fig. 1.4. Schematic diagram of creation of free volume: (a) atom squeezed into neighboring hole of smaller volume, (b) individual atomic jump for macroscopic diffusion and flow.

(b) Shear transformation zone:

Shear transformation zone (STZ), subjected to shear as shown in Fig. 1.5 resulting in strain is a small cluster of randomly close-packed atoms that spontaneously and cooperatively reorganize under the action of an applied shear stress and is considered as the fundamental unit of plastic deformation in metallic glasses. An STZ cannot be identified in a structure, however, can be detected from the change in the structure due to straining or with time. Further, theories suggested that STZ operation was strongly influenced by the local atomic arrangements and hence influences the structural evolution during deformation.

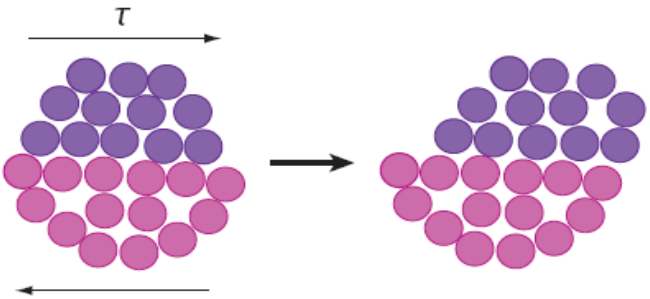

Fig. 1.5. Schematic of the two-dimensional shear transformation zone subjected to shear stress τ resulting in shear displacement with darker upper atoms moving with respect to lower atoms [6].

1.7 Role of Computational Approach in Metallic Glasses:

Now-a –days, computational approach is gaining popularity in studying various aspects of metallic glasses mainly because of following reasons:

- Through computation ,we can study both macroscopic and also microscopic aspects of deformation of metallic glasses e.g. analysis can be done at atomistic level starting from crack initiation to fracture, and also we can see the development of voids and structural changes which is not so clear from laboratory experiments.
- It also saves time and energy as through computation we can analyse everything by using proper software.
- Some metallic glasses require very high cooling rate which is very difficult to achieve practically, but they can be analyzed through simulation.

So in this project work, our main objective is to study the deformation behavior of $Cu_{50}Zr_{50}$ metallic glasses through molecular dynamics simulation studies. This sample has been chosen because of its high glass forming ability.

Chapter-2

Literature Review

2. Literature Review:

Shin Takeuchi, and Keiichi Edagawa [8] from Tokyo University of Science, Kagurazaka, Japan & Institute of Industrial Science, The University of Tokyo, Tokyo, Japan have studied on Atomistic simulation and modeling of localized shear deformation in metallic glasses.

This paper discusses atomistic simulation studies of deformation processes in metallic glasses, i.e., local shear transformation (LST), structural characterization of the local shear transformation zones (STZs), deformation-induced softening, shear band formation and its development, by use of elemental and metal–metal alloy models.

In crystalline materials, the mechanism of plastic deformation by slip process is well established by the theory of dislocation. In contrast, we have no appropriate experimental technique to detect localized stress distributions and localized structural changes in amorphous structure, because of the lack of structural periodicity. The atomistic simulation is the only available method to approach the atomistic process of the Shear band formation. They have studied stress-strain curve for shear deformation and have found that stress-strain curves show more or less serrated feature with the amplitude being larger for smaller model size. This indicates that the plastic deformation takes place discontinuously as successive localized deformation events.

Malandro and Lacks [9] have investigated the system size effect of shear deformation in a monatomic model metallic glass. They showed that the number of atoms participating in each localized deformation event increases with the system size and levels off at 50 ± 30, and the average shear flow stress decreases rapidly with increasing model size to the leveling-off stress of 0.04G.

In well-aged or slowly cooled model metallic glasses, the stress-strain relation shows a yield drop followed by a steady flow of nearly constant flow stress whereas in quenched or rapidly cooled samples, yielding occurs without upper yielding and their steady-state flow stress is nearly the same as the steady-state flow stress of the aged sample of the same model. The well-aged sample which has been pre-deformed to the steady flow stage shows no more upper yielding.

In the MD simulations, the cooling rates of the samples are 10^{9}-10^{12} K/s while the fastest quenching rate in experiments is known to be 10^{6} K/s. The structure produced by such high quenching rate used in the simulations cannot be expected from experiments. High temperature simulations showed that the flow stress decreases monotonically with increasing temperature. Regarding strain-rate effects, research shows that upper yielding in stress-strain curve is more likely to occur for faster strain-rate and the steady flow stress also increases with increasing strain-rate of the order of 10^{7}–10^{10} s^{-1}. It should be noticed that the strain-rates in the simulations are almost ten orders of magnitude higher than that of usual experiment, and the simulation results cannot be compared with the strain-rate effect in experiments.

Shigenobu Ogata, Masato Wakeda, and YojiShibutani [10] from department of mechanical engineering & department of materials science engineering, Osaka University have studied atomistic simulation of shear localization in Cu-Zr bulk metallic glasses. They have found that both the hydrostatic stress and the stress normal to the shear plane should affect the shear response.

$Cu_{57}Zr_{43}$ BMG structures were generated using the melt-quench procedure. To identify super-cell size effect, three different model sizes and shapes were considered. Simple affine shear deformation to these cells was applied by changing the super-cell basis vectors directly, according to a prescribed shear strain schedule. A stepwise increment of engineering shear strain of 0.1% was used, and relaxed the atomic configurations at each strain step by the steepest descent method.

Generally if a normal stress is affected by the shear strain, then the shear response will be affected by the normal strain. The above simulation results suggest that not only the normal stress to the sliding plane, but also the hydrostatic stress will significantly affect the shear stress response. Regarding stress-strain curve, they found that before the shear stress reaches its maximum, we see local atomic structure rearrangements at 7–11% engineering strain, because the shear deformation induces local instabilities. Correspondingly, few small shear stress drops can be found in the stress-strain curve. Shear sliding is found to occur mainly by breaking Cu–Cu bonds.

A.V. Sergueeva, N.A. Mara, D.J. Branagan, and A.K. Mukherjee [11] from Chemical Engineering and Material Science Department, University of California have studied the effect of strain rate on the ductility of metallic glasses.

Microscopic plasticity of metallic glasses during inhomogeneous deformation at room temperature is a result of a summation of local strains inherent to every shear band in the gage section. In the tests exhibiting multiple shear banding at relatively high strain rate (10^{-1} s^{-1}), an increase in ductility was also observed.

An increase in ductility during tensile test of Dy_3Al_2 metallic glass was observed at strain rate of 10^{-1} s^{-1}. Multiple parallel shear bands were observed on the gage and fracture surfaces in this case in contrast to the samples tested at lower strain rates. When lower strain rates were applied, secondary shear bands and cracks were detected in the narrow volume fraction near to fracture surface. These shear bands and cracks considered to be formed during crack propagation along primary shear band. The formation of multiple shear bands in whole volume of the sample gage has been proposed as the reason for enhanced microscopic ductility observed at the high strain rate of 10^{-1} s^{-1}.

C.Duhamel, J.Das, S.Pouly, K.S.Lee and J.Eckert [12] from different countries have studied the deformation behavior and fractographic features of ductile $Cu_{47}Zr_{47}A_{l6}$ bulk metallic glass. In this paper, the mechanical properties of a $Cu_{47}Zr_{47}A_{l6}$ BMG were reported. The deformation behavior was studied in compression under two different strain rates. SEM investigations of the fracture surfaces of the deformed samples were carried out and the observed features were correlated to the macroscopic ductility.

The amorphous alloy exhibits high strength, enhanced ductility and work-hardening. The yield strength and plastic deformation were found to be strain rate sensitive. Examination of the fracture surfaces reveals different features, depending on the overall ductility of the deformed sample.

When plastic deformation increases, the area covered by vein-like patterns decreases and new features such as river-like patterns or smooth regions appear. The surfaces of the deformed samples show that multiple shear banding occurs during deformation. Protuberances, with a 30 μm – 40 μm diameter and that interact strongly with shear bands, were found at the surface of the deformed amorphous samples.

Z.F. Zhang, J. Eckert, and L. Schultz [13] from IFW Dresden, Institute for Metallic Materials, Germany have studied the difference in compressive and tensile fracture mechanisms of $Zr_{59}Cu_{20}Al_{10}Ni_8Ti_3$ bulk metallic glass. As in most metallic glasses, $Zr_{59}Cu_{20}Al_{10}Ni_8Ti_3$ displays a different deformation and fracture behavior under compressive and tensile loading.

Under compression, the metallic glass displays some plasticity before fracture. The fracture angle θ_C between the stress axis and the fracture plane is 43°. Under tensile loading, however, the metallic glass always displays brittle fracture without yielding. The tensile fracture angle θ_T (=54°) between the stress axis and the fracture plane is larger than 45°. Therefore, both θ_C and θ_T deviate from the maximum shear stress plane (45°), indicating that the fracture behavior of the metallic glass under compressive and tensile load does not follow the von-Mises criterion.

Fracture surface observations reveal the difference in the fracture mechanisms induced compressive and tensile load. Under compression, the fracture surface only consists of a quite uniform vein-like structure. However, a combined fracture feature of veins and some cores was observed on the tensile fracture surfaces. The difference in the fracture mechanisms of the metallic glass is attributed to the effect of the normal stress on the fracture process. It is considered that the radiating cores on the fracture surface are produced by the normal tension stress in the initial stage of fracture; the veins are mainly created by the shear stress during rapid shear propagation. However, the compressive fracture of metallic glass should be mainly controlled by the shear stress. Due to the different effect of the normal stress on the fracture processes under compressive and tensile load, the deviation of θ_C and θ_T from 45° shows a large difference.

Chapter-3

Computational Methods

3.1 Molecular Dynamics Simulation

3.1.1 Introduction:

Molecular dynamics (MD) is a computer simulation technique where the time evolution of a set of interacting atoms and molecules of a system is followed by integrating their equations of motion. The atoms and molecules of the system are allowed to interact for a period of time giving a view of their motion. The trajectories of the interacting particles are determined by numerically solving Newton's equations of motion where forces between the particles and potential energy are defined by molecular mechanics force fields. The Newton's equation of motion can be expressed mathematically as follows:

$$F = m_i a_i \quad \ldots\ldots\ldots\ldots\ldots\ldots\ldots\ldots\ldots\ldots\ldots\ldots (1)$$

$$a_i = d^2 r_i / dt^2 \quad \ldots\ldots\ldots\ldots\ldots\ldots\ldots\ldots\ldots\ldots\ldots\ldots (2)$$

Where F = force between the interacting particles

m_i = mass of each particle (considering a homogeneous system, mass of each particle is same)

a_i = Acceleration of each particle

r_i = particle position

Given an initial set of positions and velocities, the subsequent time evolution through which the particle interaction and movement takes place can be completely determined. During simulation atoms and molecules will 'move' in the computer, bumping

into each other during interaction, vibrating about a mean position (if constrained), or wandering around (if the system is fluid), oscillating in waves in concert with their neighbors, perhaps evaporating away from the system if there is a free surface, and so on, in a way similar to what real atoms and molecules would do.

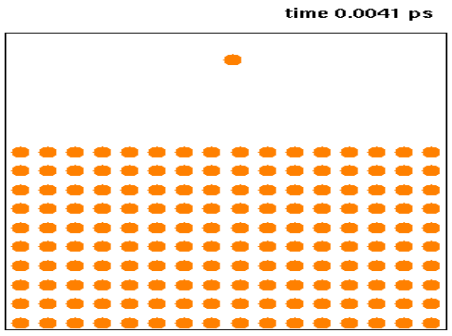

Fig. 3.1. Example of a MD simulation in a simple system: Deposition of a single Cu atom over a Cu (001) surface. Each colored atom represents Cu atom [1]

Since any molecular system contains a large no of micro-particles, atoms or molecules, so it is not possible to characterize the properties of such a vast system analytically, In this case MD simulation approaches this problem by using numerical methods. In order to get simulation results to be error free, calculations are carried out by the machine (computer) selecting a proper algorithm implemented in a suitable programming language. In this way, complexity can be introduced and more realistic systems can be investigated, achieving a better understanding of real experiments. Due to its important commercial applications, this simulation technique is now gaining much more popularity. The method was originally conceived within theoretical physics in the late 1950s and early 1960s, but is applied today mostly in materials science and the modeling of bio-molecules.

3.1.2 Mechanism & Design Parameters:

MD simulation facilitates the study on the dynamics of large macro-molecules along with the optimization of resulting structures. The trajectory obtained by molecular dynamics as per the algorithm provided gives a set of conformations of molecule. First, atoms and molecules interact with each other. These interactions are due to forces which act upon each and every atom, and which originates from all other atoms by giving them a certain initial momentum. Atoms move under the action of these instantaneous forces. As the atoms move, their relative positions change and forces change as well.

Typical MD simulations are performed on systems containing thousands of atoms. To start the simulation, first a set of initial positions and velocities are created for the atoms in the molecule. The initial positions usually correspond to a known structure (from X-ray or NMR structures, or predicted models). The initial velocities are then assigned taking them from a Maxwell distribution at a certain temperature T to initiate atomic movements. Another possibility is to take the initial positions and velocities to be the final positions and velocities of a previous MD run. As the simulation proceeds with atomic movements, thermodynamic parameters of the system like temperature, pressure, volume, total energy also changes and finally we get the desired result as per the algorithm used. Based on these parameters, simulation can be done in various ways. They are as follows [14]:

Micro-canonical or NVE ensemble:

In this case, the system is restrained from changes in moles (N), volume (V) and energy (E). It corresponds to an adiabatic process with no heat exchange. A micro-canonical molecular dynamics trajectory may be considered as an exchange of potential and kinetic energy, with total energy being conserved.

Canonical or NVT ensemble:

In this case, moles (N), volume (V) and temperature (T) are conserved. It is also sometimes called constant temperature molecular dynamics (CTMD). In NVT, the energy of endothermic and exothermic processes is exchanged with a thermostat. A variety of thermostat methods is available to add and remove energy from the boundaries of an MD system in a more or less realistic way, approximating the canonical ensemble.

Isothermal–Isobaric or NPT ensemble:

In this case, moles (N), pressure (P) and temperature (T) are conserved. In addition to a thermostat, a barostat is needed to control the pressure to approximate real situation.

Design of a molecular dynamics simulation should be in accordance with available computational power. Parameters like simulation size (n=number of particles), timestep and total time for simulation must be selected so that the calculation can be finished within a reasonable time period. To make statistically valid conclusions from the simulations, the simulation time should match the kinetics of the natural process. Generally, simulation time ranges from a few picoseconds to hundreds of nanoseconds. A simulation is reliable when the simulation time is much longer than the relaxation time of the quantities (to attain stability or lowest energy state) we are interested in. To obtain these simulations, several CPU-days to CPU-years will be needed. Parallel algorithms are implemented for this purpose allowing the task to be distributed among CPUs; an example is the spatial or force decomposition algorithm.

Various factors affect the total simulation time and they should be taken into consideration during simulation. During a classical MD simulation, the most important task of CPU is the evaluation of the potential (force field) as a function of the particles' internal coordinates. Calculations are more time-taking, when the non-bonded or non-covalent parts of a system are encountered.

In molecular dynamics simulation, potential function or force field measures quantitatively how the particles in the simulation will interact. These potential functions represent a classical treatment of particle-particle interactions that results in structural and conformational changes but usually cannot reproduce chemical reactions. When finer levels of detail are required, potentials based on quantum mechanics are used. So various potentials that are widely used in simulation are given below and choice of potential depends on the type of material system we are dealing with.

Empirical Potentials:

Those used in chemistry are frequently called force fields, while those used in materials physics are called just empirical or analytical potentials. Most force fields in chemistry are empirical and consist of a summation of bonded forces associated with chemical bonds, bond angles, torsional forces and bond dihedrals and non-bonded forces associated with vanderWaals forces and electrostatic charge. The total potential energy can be expressed as:

$$E_{pot} = \sum V_{bond} + \sum V_{ang} + \sum V_{torsion} + \sum V_{vdW} + \sum V_{ele} + \ldots$$

Its calculation is the main culprit in the speed of MD simulations. Examples of such potentials include the Brenner potential for hydrocarbons and its further developments for the C-Si-H and C-O-H systems.

Pair wise Potentials & Many-Body Potentials:

In pair wise potentials, the total potential energy is calculated from the sum of energy contributions between pairs of atoms. An example of such a pair potential is the non-bonded Lennard–Jones potential used for calculating van der Waals forces.

In many-body potentials, the potential energy includes the effects of three or more particles interacting with each other. In simulations with pairwise potentials, global interactions in the system also exist, but they occur only through pairwise terms. In many-body potentials, the potential energy cannot be found by a sum over pairs of atoms, as these interactions are calculated explicitly as a combination of higher-order terms. For example, the Tersoff potential, which was originally used to simulate carbon, silicon and germanium and the most widely used embedded-atom method (EAM).

Semi-Empirical Potentials:

It makes use of the matrix representation from quantum mechanics. The matrix is then diagonalized to determine the occupancy of the different atomic orbitals, and empirical formulae are used to determine the energy contributions of the orbitals.

Polarizable Potentials:

It includes the effect of polarizability, e.g. by measuring the partial charges obtained from quantum chemical calculations. This allows for a dynamic redistribution of charge between atoms which responds to the local chemical environment. For systems like water and protein better simulation results obtained by introducing polarizability.

Ab-initio Quantum-Mechanical Methods:

Ab-initio calculations produce a vast amount of information that is not available from empirical methods, such as density of electronic states or other electronic properties.

A significant advantage of using *ab-initio* methods is the ability to study reactions that involve breaking or formation of covalent bonds, which correspond to multiple electronic states.

Another parameter that affects total CPU time required by a simulation is the size of the integration timestep. This is the time length between evaluations of the potential function. The time step must be chosen small enough to avoid discretization errors (i.e. smaller than the fastest vibrational frequency in the system). Typical time steps for classical MD are in the order of 1 femtosecond (10^{-15} s). Proper time integration algorithm should be implemented to achieve optimum simulation time.

Time integration algorithms are based on finite difference methods, where time is discretized on a finite grid, the time step Δt being the distance between consecutive points on the grid. Knowing the positions and some of their time derivatives at time t, the integration scheme gives the same quantities at a later time $t+\Delta t$. By iterating the procedure, the time evolution of the system can be followed for long times. The schemes are approximate and there are errors associated with them which can be reduced by decreasing Δt.

Two popular integration methods for MD calculations are the Verlet algorithm and predictor-corrector algorithms. The most widely used time integration algorithm is the Verlet algorithm. In this case, the position of a particle at any time t is given by:

$$V(t) = \{r(t+\Delta t) - r(t-\Delta t)\}/2\Delta t \quad \text{.....(3)}$$

Where $V(t)$ = Velocity of a particle at time t.

$R(t)$ = position of a particle at time t.

Δt = Small change in time.

The predictor-corrector algorithm consists of three steps

- Step 1: Predictor: From the positions and their time derivatives at time t, one 'predicts' the same quantities at time $t+\Delta t$ by means of a Taylor expansion. One such quantity is acceleration.
- Step 2: Force evaluation: The force is computed by taking the gradient of the potential at the predicted positions. The difference between the resulting acceleration and the predicted acceleration gives error.
- Step 3: Corrector. This error signal is used to 'correct' positions and their derivatives. All the corrections are proportional to the error signal, the coefficient of proportionality being determined to maximize the stability of the algorithm.

In all kinds of molecular dynamics simulations, the simulation box size must be large enough to avoid surface effects. Atoms near the boundary have fewer neighbours than atoms inside resulting surface effects in the simulation to be much more important than they are in the real system. Boundary conditions are often treated by choosing fixed values at the edges (which may cause surface effects), or by employing periodic boundary conditions where the particles interact across the boundary and can move from one end to another end.

3.1.3 Applications of MD simulation [1]:

- It is mostly used for simulation of bio-molecular systems like protein synthesis and characterization.
- Used for drugs designing in pharmaceutical industry to test properties of a molecule without synthesizing it.
- Used to study the effect of neutrons and ion irradiation on solid surfaces.
- It has wide applications in materials sectors too where experiments regarding any problem are very difficult to carry out in laboratory conditions.
- It is also used to study various properties of metals, non-metals and alloys like fatigue properties, tensile properties, deformation behavior, high temperature behavior etc.

3.2 LAMMPS & VMD [13]:

- LAMMPS is a classical molecular dynamics code and an acronym for Large-scale Atomic/Molecular Massively Parallel Simulator. This is the basic code required to do materials simulation.
- LAMMPS has potentials for soft materials (bio-molecules, polymers) and solid-state materials (metals, semiconductors) and coarse-grained or mesoscopic systems.
- It can be used to model atoms or as a parallel particle simulator at the atomic, meso, or continuum scale.
- LAMMPS runs on single processors or in parallel using message-passing techniques and a spatial-decomposition of the simulation domain**.**
- LAMMPS is an open source code distributed by Sandia National Laboratories, a US Department of Energy laboratory. This code is written with the help of c++.

The designing structure of the code is so flexible that it can be easily modified and extended with new applications.

- It uses many of the force fields or potentials described in section 3.1.2. It is highly compatible with the design parameters and mechanism of simulation described in section 3.1.2.
- A set of pre- and post-processing tools are also packaged with LAMMPS, some of which can convert input and output files to/from formats used by other codes.
- VMD is a molecular visualization program for displaying, animating, and analyzing large biomolecular systems using 3-D graphics and built-in scripting.
- It supports all computer platforms, processors and not limited by no of particles in the system under observation except available computational memory.
- It is open source code.

In our project work, all the simulations have been done using LAMMPS code and resulting models and structures have been analyzed using VMD Visualization programme.

3.3 Simulation Procedures

3.3.1 Procedures:

- In order to do simulation, first we have to install LAMMPS software in our personal computer.
- We need three basic program files for any simulation. They are:
    a) In .file (program file to create models and doing simulation)
    b) Potential file(contains data about inter atomic bond energy between atoms)
    c) Exe file (required to run the commands in the in.file

Apart from these files, to study deformation we need a data file containing prior Atomic coordinates of the amorphous structure.

- Then next step is to open command prompt screen (dos environment) by typing "cmd" in start icon.

- In the displaying screen, the default directory will be displayed as "C:\users\name of the computer>"(For ex: C:\users\dell>). If the above said programme files are in another directory, we have to change the path directory by typing in the screen as "C:\users\name of the computer>directory name: enter"(for ex: C:\users\dell>E:enter). Then our desired directory name will be displayed as "directory name :\>". (For ex: E:\>).
- Then type as E:\>cd "path address of the above programme files in the LAMMPS folder" then press enter. Then the screen will display the same path address. After that next to the path address type as: "Path address > lmp_win_no-mpi.exe<in.file name" then press enter. Then automatically the in.file will be executed by the .exe file and if there is any error in the in.file then it will be displayed in the command prompt screen and after rectification of all the errors, the output values will be displayed.

3.3.2 Output of Simulation:

- After successful running of the in.file, we will get four out-put files as follows:
    a) DUMP file (containing the atomic co-ordinates of the final structure after simulation and also for deformation studies it contains the stress component values).

b) RDF file (contains co-ordination values of atoms and radial distribution function values). RDF or radial distribution function is a measure of arrangement of atoms in the material.

c) Log file (contains thermodynamic data e.g temperature, pressure, volume, and total energy after a particular no of steps).

d) Log. lammps file

- Now to see the final structure after simulation, we have to open dump file that contains atomic co-ordinates, through VMD software which need to be installed in the system.
- VMD has three parts.

a) VMD main

b) Display screen

c) Programme screen

Necessary adjustments to the final structure like change of color, display format (Atomic or point etc) can be done through VMD main. In display screen we see the image of the final structure. In the programme screen, any changes that we do in VMD main and final results are displayed.

Chapter-4

Results & Discussions

During the execution of this project work, the various simulations and analysis that has been carried out are as follows:

a) Creation of $Cu_{50}Zr_{50}$ alloy models of different sizes and subsequent quenching at significantly high cooling rate to get glassy structures.
b) Study of various thermodynamic parameters during quenching like Volume-temperature relation and structural characterization such as RDF plots.
c) Uniaxial tensile deformation of the quenched $Cu_{50}Zr_{50}$ specimens along y-direction at 300 K. Also the effect of strain rate and cross-section size has been studied.
d) Distribution of shear stress and normal tensile stress on the atoms has been studied through contour plots.
e) Fracture behavior of $Cu_{50}Zr_{50}$ amorphous alloy model.

4.1 Creation of Cu_{50} Zr_{50} alloy models & quenching procedure

Here the purpose of simulation is to create a $Cu_{50}Zr_{50}$ glassy model e.g. a amorphous structure by first heating a crystalline model of same alloy up to the melting temperature 2300 K, then holding it for sufficient time to complete phase transformation from solid state to liquid state, then finally quenching the model at a very high cooling rate up to the room temperature 300 K to get the desired amorphous or glassy structure.

The in.file which contains all the commands to create a model and to quench it at a particular cooling rate is given below.

 # In.file (for size X=50Å, Y=30Å, Z=20Å & cooling rate 10^{14} K/s):

```
units           metal
echo            both
atom_style      atomic
dimension       3
boundary        p p p

region          box block 0 50 0 30 0 20  units box

create_box      2 box

lattice         fcc 3.61
region          cu block 0 50 0 30  0 20 units box
create_atoms    1 region cu units box
# creating composition using set command for cu50zr50 alloy
set             region cu type/fraction 2 0.5 12393

timestep        0.002
pair_style      eam/fs
pair_coeff      * * Cuzr_mm.eam.fs Cu Zr
# Energy Minimization
minimize        1.0e-4 1.0e-6 100000 100000
thermo          100
thermo_style    custom step temp vol press etotal
dump            1 all atom 1000 5050_q_3d_s.dump.lammpstrj  id type  x  y  z vx vy vz
#dump_modify    1 scale no
log             log5050_q_3d_s.data
```

```
velocity        all create 300 8728007 rot yes mom yes dist gaussian
#fixes
compute         myRDF all rdf 100
fix             1  all ave/time 100 1 100c_myRDF file Cu_zr_melt_3.rdf mode vector
fix             2 all npt temp 300.0 2300.0 0.2 iso 0.0 0.0 0.2
run             20000
fix             3 all npt temp 2300.0 2300.0 0.2 iso 0.0 0.0 0.2
run             20000
fix             4 all npt temp 2300.0 300 0.2 iso 0.0 0.0 0.2
run             10000
```

Through this in.file which is named here in.CuZr_melt (naming is user defined) along with potential file for $Cu_{50}Zr_{50}$ which is named within the in.CuZr_melt file as CuZr_mm.eam.fs and lmp_win_no-mpi.exe file, we can do the simulation. For specimens of other dimensions, the in.file should be modified by changing the dimensions in the region command.

The cooling rate is calculated by dividing the temperature difference by the total time taken for cooling. Here in this in.file, the last three commands represent the quenching step from where temperature difference can be calculated e.g.

Temp difference = 2300 K-300 K =2000 K

Total time taken for cooling = timestep × no of iterations in quenched step

= (0.002 × 10000) ps

So cooling rate = 2000 K / (0.002 × 10000) ps = 10^{14} Ks^{-1} for the above in.file

After successful running, we get the final amorphous $Cu_{50}Zr_{50}$ models of different sizes which can be seen in VMD. The VMD images of the quenched structures for different sizes are given below:

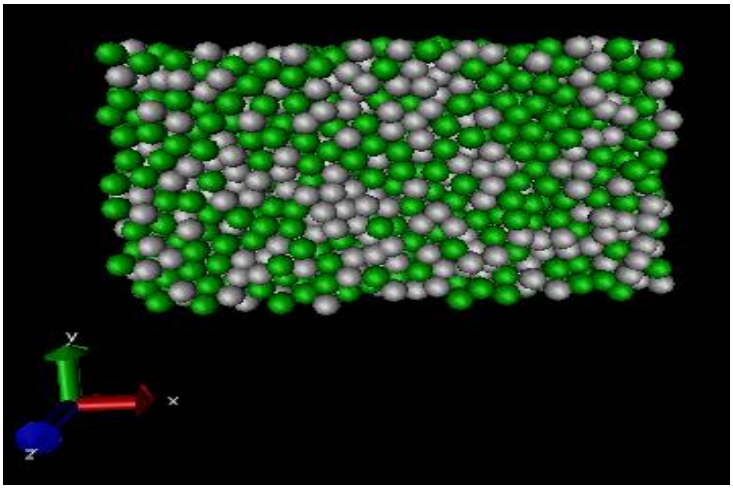

Fig. 4.1 VMD snap shot showing alloy models of Size: x=50 Å y=30 Å z=20 Å.
(No of atoms=2856)

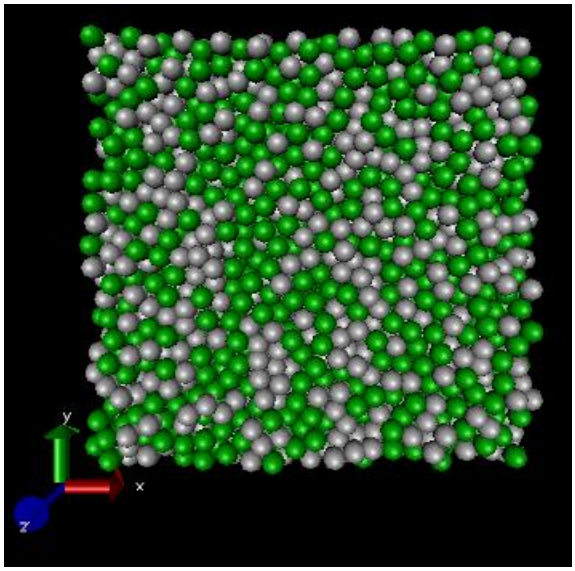

Fig. 4.2 VMD snap shot showing alloy models of Size: x=50 Å y=50 Å z=20 Å.
(No of atoms=4704)

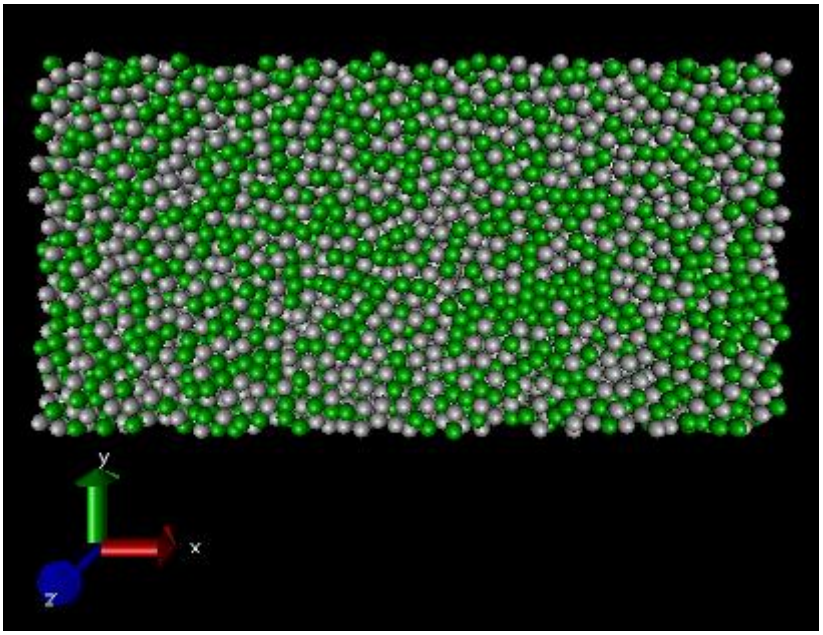

Fig. 4.3 VMD snap shot showing alloy models of Size: x=100 Å y=50 Å z=100 Å.
(No of atoms=43904)

4.2 Volume - temperature plots (for size x=100Å, y=50Å, z=100Å):

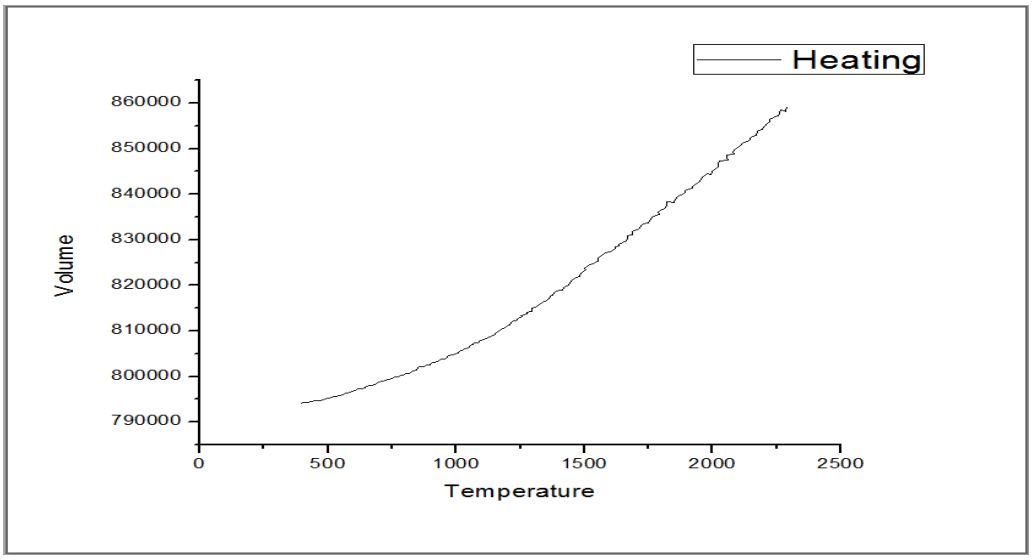

Fig. 4.4 Volume-Temperature plot during heating X-axis: Temperature (in K)
Y-axis: Volume (in $Å^3$)

So from the above plot we can see that during heating as temperature increases from room condition 300 K to 2300 K (which is the melting point of $Cu_{50}Zr_{50}$), volume also

increases as indicated by the y-axis. This behavior is same as that of crystalline metals as during heating stage the model created through simulation is actually crystalline which will become amorphous after being quenched.

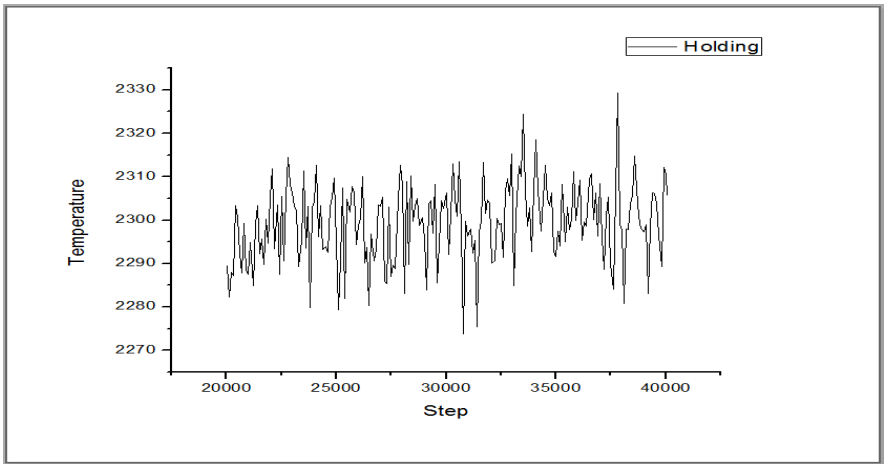

Fig. 4.5 Temperature-time during holding at temperature of 2300 K

X-axis: Step or Iterations

Y-axis: Temperature (in K)

As shown in the Fig. 4.5 phase transformation of the crystalline model created is taking place as the material melts at 2300 K. So temperature remaining constant nearly at 2300 K with slight variations as shown in the graph. During this stage, whatever energy is provided is utilized in increasing the volume, so temperature remains constant.

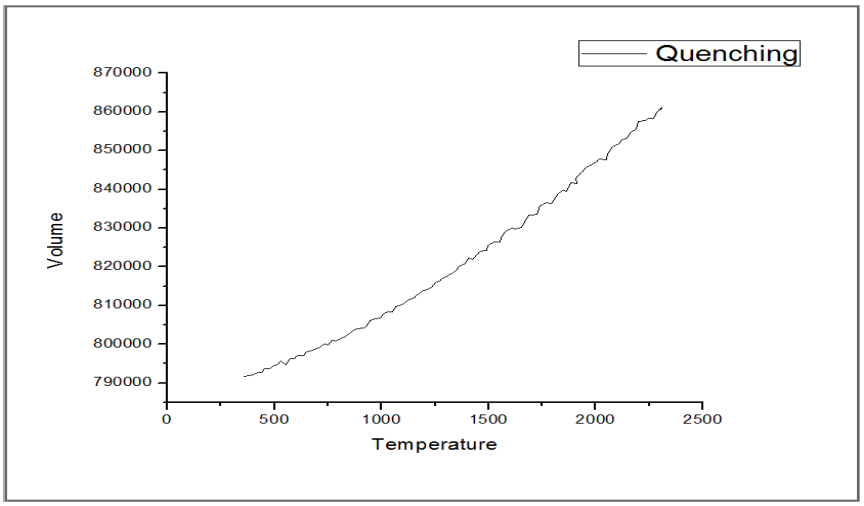

Fig. 4.6 Volume-Temperature plot during quenching at a rate of 10^{14} K/s

X-axis: Temperature (in K)

Y-axis: Volume (in $Å^3$)

This is the plot after the melt specimen is subjected to rapid quenching. Here we finally got our desired glassy model or amorphous structure after completion of quenching. This simulated result is very much similar to experimental plot.

4.3 Radial Distribution Function (RDF):

- A pair-distribution or radial function provides the probability of finding a distance "*r*" between two atoms in a material.

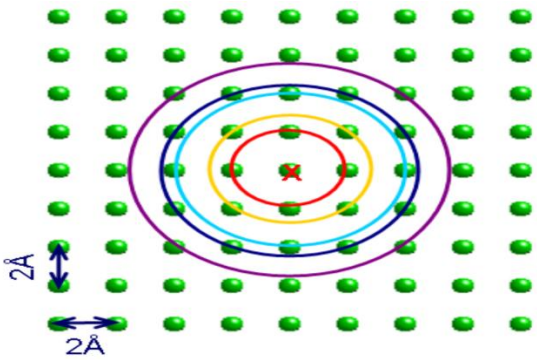

Fig.-4.7 Atomic arrangements in a crystalline material

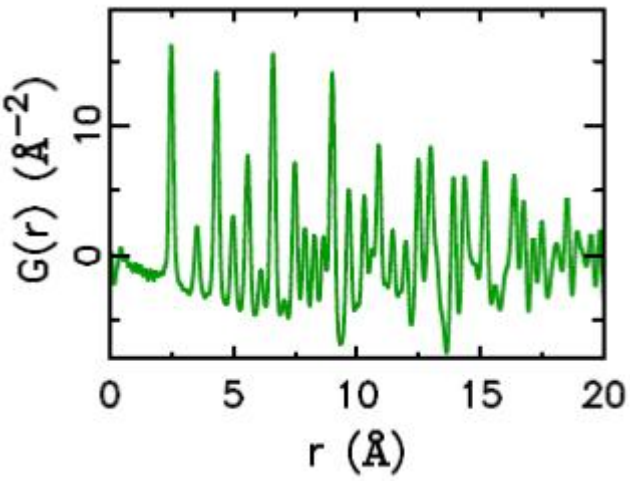

Fig.-4.8 RDF plot for a crystalline material

- The atomic RDF G(r) shows peaks corresponding to the inter-atomic distances existing in the material.
- The RDF technique is based on the total scattering – Bragg peaks and diffuse contribution – it can provide informations for both the average structure and the local atomic arrangement.
- It allows for a direct analysis of the inter-atomic distances and atomic displacements without prior knowledge of the structure.
- It also gives a measure of crystalline nature of a material. Crystals are close packed structures. So more is the close packing, more peaks of higher values will be observed at lower radial distances. For amorphous structure, no of peaks will be less and peak value will be lower.

RDF plots (for size x=100Å, y=50Å, z=100Å):

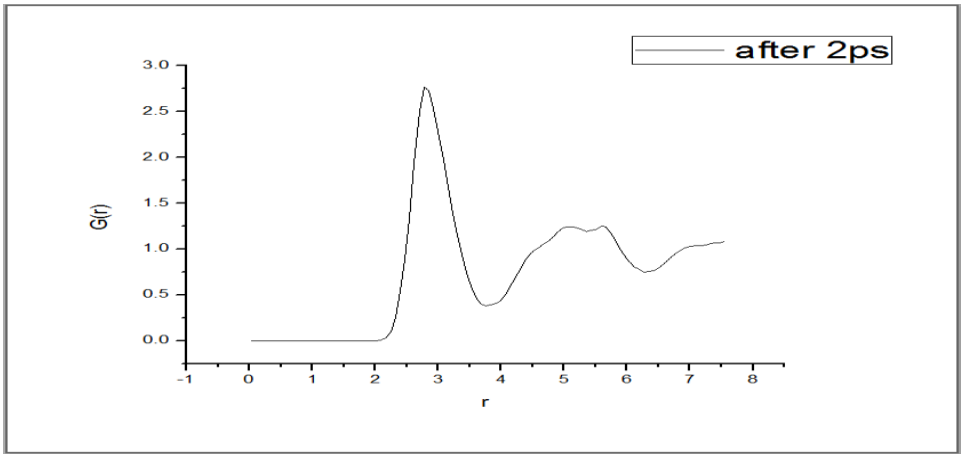

Fig. 4.9 RDF plot during heating after 2ps of simulation

X-axis: radial distance r (Å)

Y-axis: RDF G(r) [in $Å^{-2}$]

As shown in the Fig. 4.9, the specimen model created is still crystalline and undergoing heating stage. So at a radial distance up to 2Å the probability of finding two atoms is zero. Maximum probability is in between 2 Å to 4 Å, then probability again shows some down and up behavior. Since crystal is a close packed structure, maximum probability is exceeding 2.5 for the radial distance from 2 Å to 4 Å.

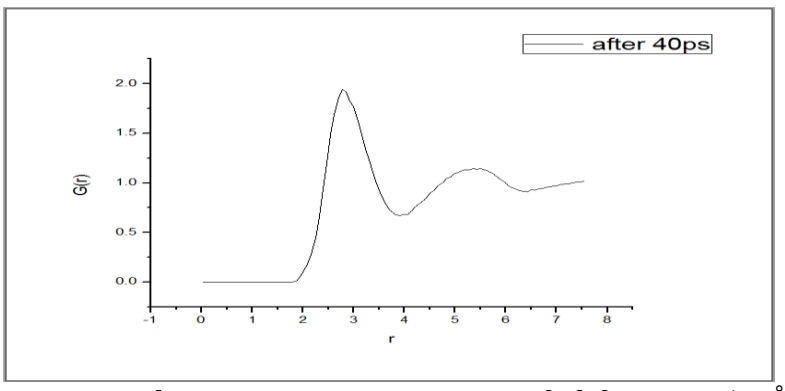

Heating complete X-axis: radial distance r (in Å)

Y-axis: rdf G(r) [in $Å^{-2}$]

Fig. 4.10 RDF plot after 40ps of simulation

In Fig. 4.10 similar interpretation can be done like Fig. 4.9. Since after this, melting will start, atoms are less close-packed here. So maximum probability that is in between 2Å to 4Å is below 2.

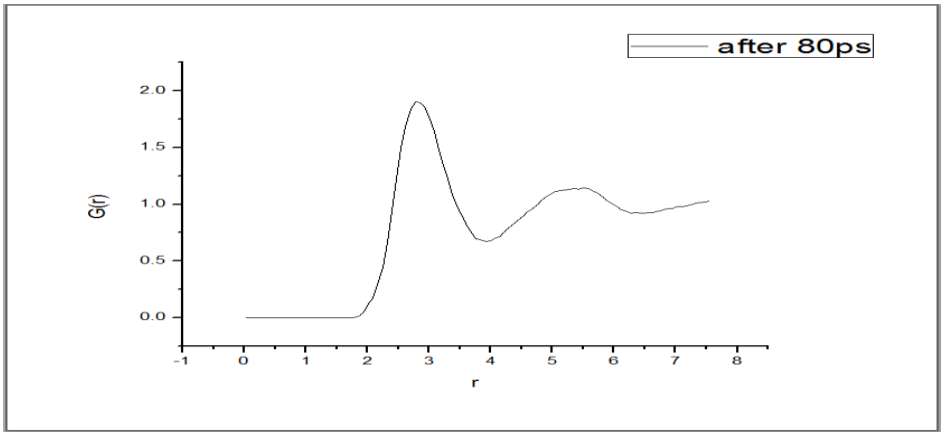

Melting complete X-axis: radial distance (in Å)

Y-axis: RDF G(r) [in $Å^{-2}$]

Fig. 4.11 RDF plot after 80ps of simulation

In Fig. 4.11, the sample is fully liquid. There is no close packing here. So, maximum probability is much lower (below 2) in comparison to Fig. 4.10.

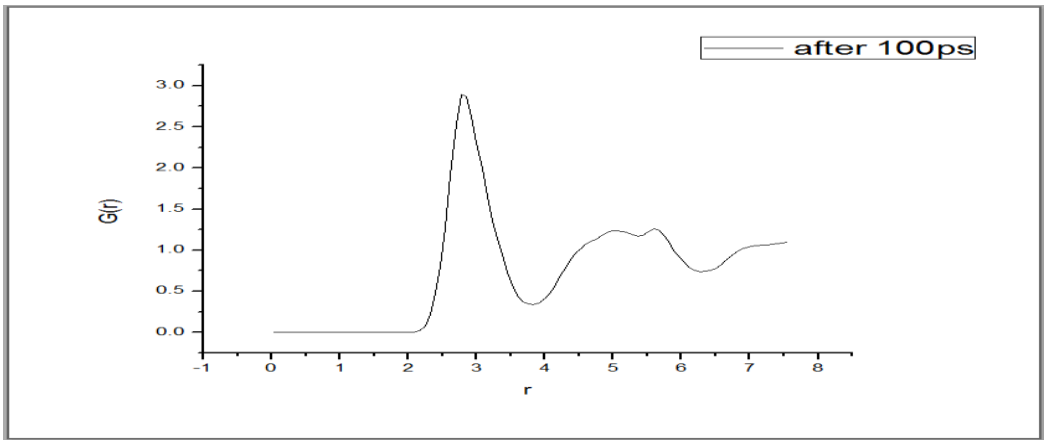

Quenched or amorphous structure X-axis: radial distance r (in Å)

Y-axis: RDF G(r) [in $Å^{-2}$]

Fig. 4.12 RDF plot of the quenched structure after 100ps of simulation

In Fig. 4.12, the quenched sample is again super cooled liquid, so maximum probability again exceeds 2.5. Since, it is amorphous in nature, so due to random arrangement of atoms, the maximum probability is less in comparison to Fig. 4.9 where the structure is crystalline.

4.4 Tensile Deformation of Quenched Specimens:

Computational Steps:

a) We need 4 files to run tensile deformation simulation program namely in.file, read_data file, potential file and lammps.exe file in a single folder.

b) Read_data fie contains the atomic co-ordinates of the atoms of the quenched specimen and this file can be created from the data in last iteration step in dump file obtained after simulation of quenching.

c) Output files are dump file, dump.stress file, log file, log.lammps file.

d) Dump.stress file gives six components of stress tensor in the order σ_x, σ_y, σ_z, τ_{xy},τ_{xz} ,τ_{yz} where only σ_y will be used to plot Stress Vs Strain curve .

Here the purpose of simulation is to do uniaxial tensile deformation of the quenched specimen along y-direction. Below is the in.file that contains all the commands required to do simulation of tensile deformation. First the deformation was carried out for different sizes at a particular strain rate, then for a particular size at different strain rates and stress-strain plots were drawn.

To do deformation for different sizes at a particular strain rate, read data file was changed according to the size concerned by accessing the data in the dump file obtained after

simulation of quenching. . Similarly, to do deformation at different strain rates for same size the strain rate which is mentioned as 'erate' in the in.file was changed accordingly.

 # In.file for 3d tensile simulation (at strain rate 10^{11} s^{-1}):

```
units           metal
dimension       3
boundary        p pp
atom_style      atomic
echo            both
read_data       5050_1crystal_3d_large_tensile.dat
timestep        0.001
pair_style      eam/fs
pair_coeff      * * Cuzr_mm.eam.fs  Cu Zr
# Energy minimization
minimize        1.0e-5  1.0e-10  10000  100000
dump            1 all atom 100 dump.uniaxialtensile8_3d_l_one_crystallites.dump.lammpstrj
log             log5050_uniaxialtensile8_3d_l_one_crysatallites.dat
# initial velocities
velocity        all create 298  482748  rot yes mom yes dist gaussian
Fix             1 all deform 100 y erate 0.1
fix2            all npt temp 300.0 300.0 100.0 x 0 0 100.0 z 0 0 100.0   dilate all
fix3            all temp/rescale 100 300 300 0.05 1.0
compute         1 all stress/atom
thermo          100
thermo_style    custom step temp press vol etotal
```

```
dump        2 all custom 100 dump.stress_atom_uniaxialtensile8_3d_l_one_crystallites c_1[1]
            c_1[2] c_1[3] c_1[4] c_1[5] c_1[6]
run         1000
```

Structure of $Cu_{50}Zr_{50}$ before and after tensile deformation:

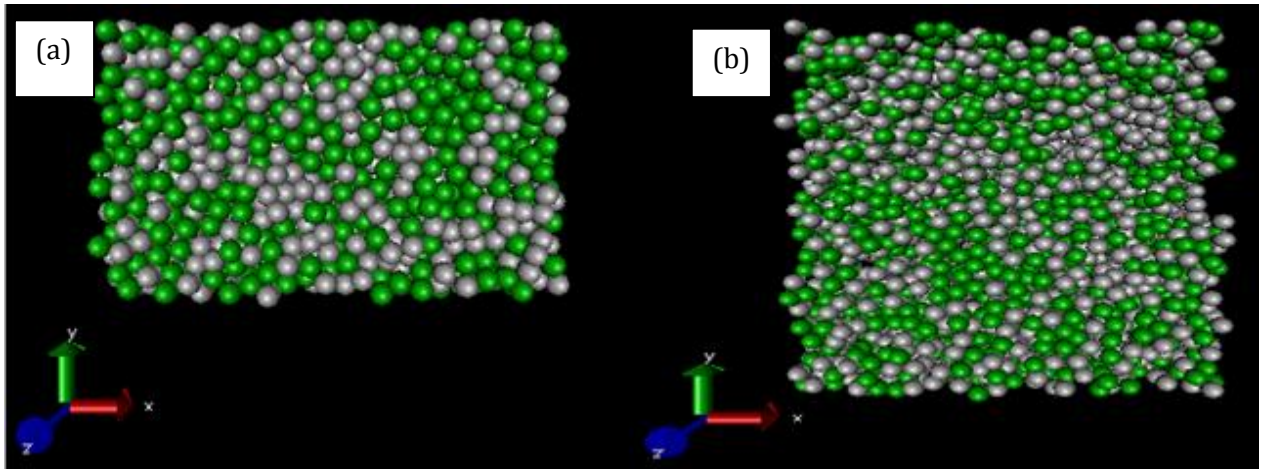

Fig. 4.13 Structure of alloy model before and after tensile deformation: (a) Structure of alloy model before uniaxial tensile deformation; (b) Structure of alloy model after uniaxial tensile deformation. Size: X=100Å Y=50Å Z=100Å

As from the above figure, we can observe the change in the structure (we are doing tensile deformation in Y-direction, so dimension was increased in that direction)

Stress-Strain plots for different sizes of alloy at same strain rate 10^{11} s^{-1}:

Table 4.1: Stress-strain data for size 50Å × 30Å × 20Å (2856 atoms) at strain rate of 10^{11} s^{-1}

Stress (GPa)	Strain
0.125347	0.01
0.802853	0.02
1.5232	0.03
2.278453	0.04
3.02736	0.05
3.7128	0.06
4.3792	0.07
4.880587	0.08
5.590715	0.09
6.0928	0.1

Based on the data given in Table 4.1, the stress-strain plot obtained has been shown below:

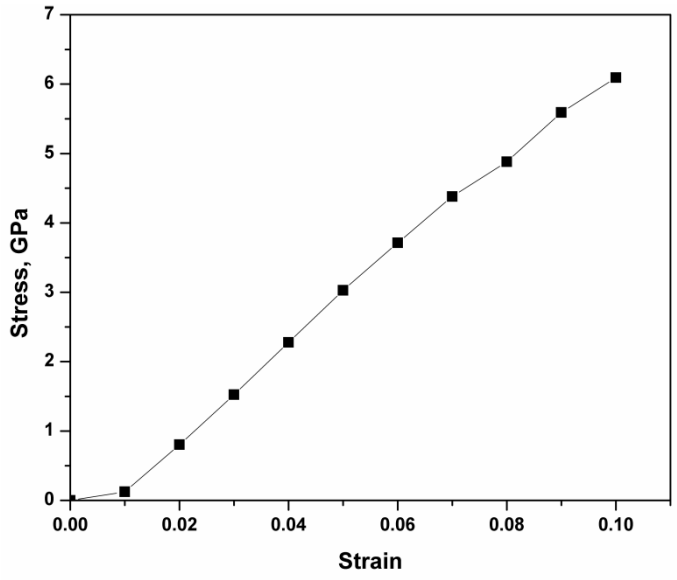

Fig. 4.14: Engineering stress-engineering strain plot for size 50Å × 30Å × 20Å (2856 atoms) at strain rate of 10^{11} s^{-1}.

Table 4.2: Stress-strain data for size 50Å × 50Å × 20Å (4704 atoms) at strain rate of 10^{11} s^{-1}

Stress (GPa)	Strain
0.23567	0.01
0.90508	0.02
1.6561	0.03
2.44453	0.04
3.05446	0.05
3.73184	0.06
4.35904	0.07
4.89216	0.08
5.42528	0.09
5.9584	0.1

Based on the data given in Table 4.2, the stress-strain plot obtained has been shown below:

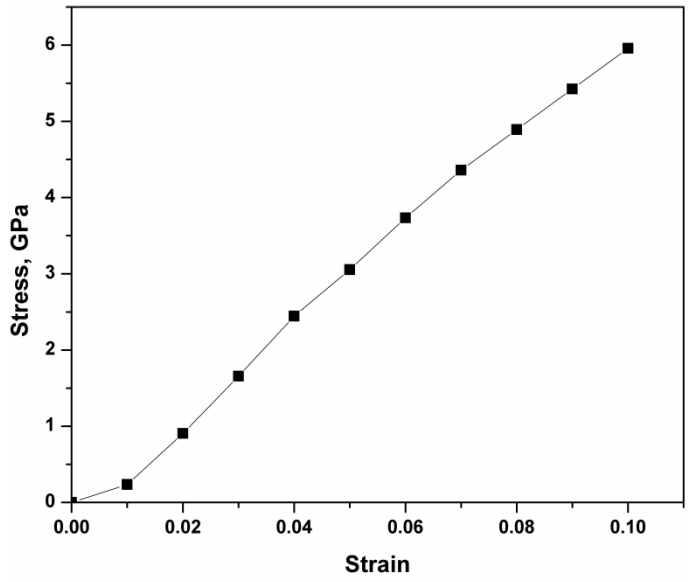

Fig. 4.15: Engineering stress-engineering strain plot for size 50Å × 50Å × 20Å at strain rate 10^{11} s^{-1}.

Table 4.3: Stress-strain data for size 50Å × 100Å × 20Å (9408 atoms) at strain rate 10^{11} s^{-1}

Stress (GPa)	Strain
0.1706	0.01
0.86945	0.02
1.62277	0.03
2.36641	0.04
3.02938	0.05
3.73184	0.06
4.37205	0.07
4.95488	0.08
5.55072	0.09
5.98976	0.1

Based on the data given in Table 4.3, the stress-strain plot obtained has been shown below:

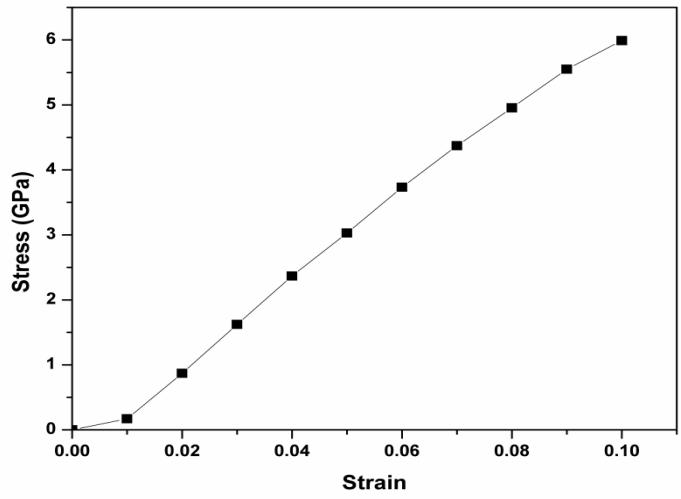

Fig. 4.16: Engineering stress-engineering strain plot for size 50Å × 100Å × 20Å at strain rate of 10^{11} s^{-1}.

Comparison of the stress-strain plots for different sizes (varying heights and cross section of the sample) at same strain rate:

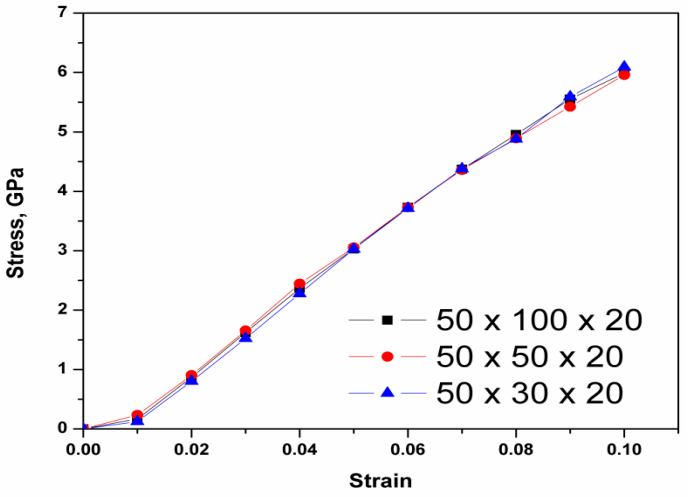

Fig. 4.17a Comparison of engineering stress-engineering strain plots for different heights of $Cu_{50}Zr_{50}$ alloy model at strain rate of 10^{11} s^{-1}.

From Fig. 4.15 and Fig. 4.18, we can have a comparison plot as shown below:

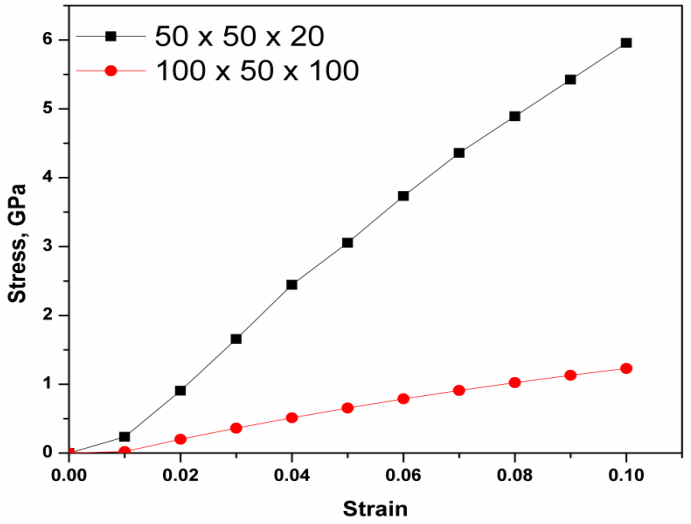

Fig. 4.17b: Comparison of engineering stress-engineering strain plots for different cross section sizes of $Cu_{50}Zr_{50}$ alloy model deformed at strain rate of 10^{11} s^{-1}.

From Fig. 4.17a we can conclude that the deformation behavior of samples with different heights at same strain rate is almost similar while that with increase in cross-section size there is significant decrease in stress with strain as shown in Fig. 4.17b.

Stress-Strain plots at different strain rates for size 100Å × 50Å × 100Å:

Table 4.3: Stress-strain data for size 100Å × 50Å ×100Å (43904 atoms) at strain rate 10^{11} s^{-1}

Stress (GPa)	Strain
0.02264	0.01
0.1996	0.02
0.36151	0.03
0.51305	0.04
0.65504	0.05
0.78894	0.06
0.90928	0.07
1.02323	0.08
1.12946	0.09
1.22931	0.1

Based on the data given in Table 4.3 the stress-strain plot obtained has been shown below:

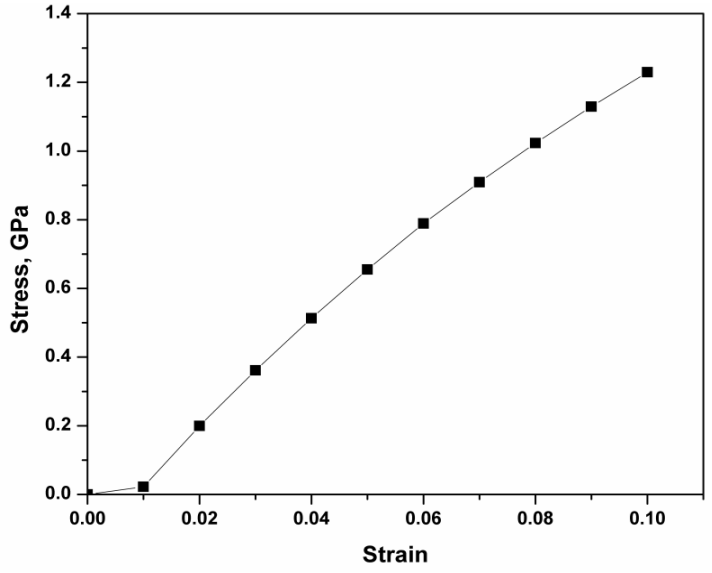

Fig. 4.18: Engineering stress-engineering strain plot for size 100Å × 50Å ×100Å (9408 atoms) at strain rate of 10^{11} s^{-1}.

Table 4.4: Stress-strain data for size 100Å × 50Å × 100Å (43904) at strain rate 10^{12} s^{-1}

Stress (GPa)	Strain
0.10566	0.1
6.5856	0.2
9.80523	0.3
10.41988	0.4
8.66372	0.5
6.29291	0.6
4.61431	0.7
3.58415	0.8
2.84377	0.9
2.36496	1

Based on the data given in Table 4.4, the stress-strain plot obtained has been shown below:

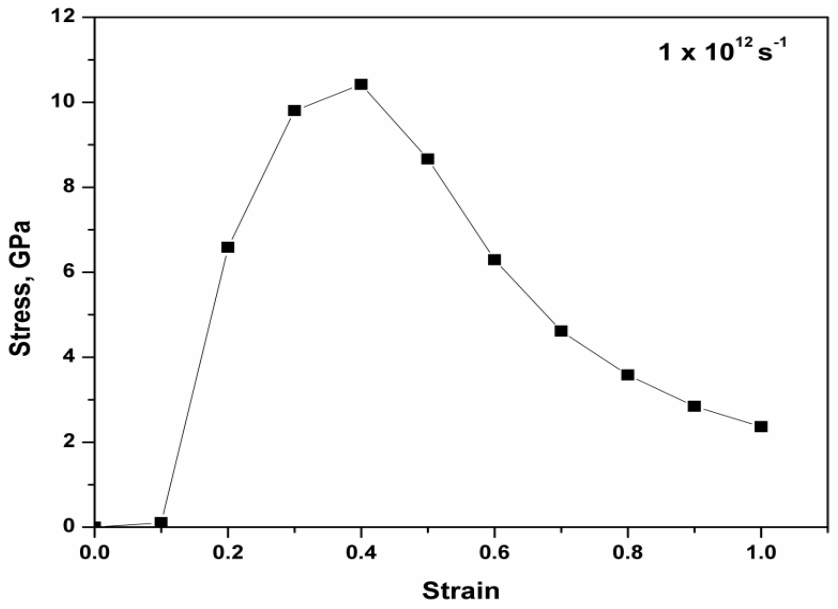

Fig. 4.19: Engineering stress-engineering strain plot for size 100Å × 50Å × 100Å at strain rate of 10^{12} s^{-1}.

Table 4.5: Stress-strain data for size 100Å × 50Å× 100Å at strain rate of 10^{13} s^{-1}

Stress in GPa	Strain
0.10566	1
6.04326	2
1.43611	3
0.69923	4
-0.17405	5
-0.0203	6
-0.40276	7
-0.25377	8
-0.44994	9
-0.34582	10

Based on the data given in Table 4.5, the stress-strain plot obtained has been shown below:

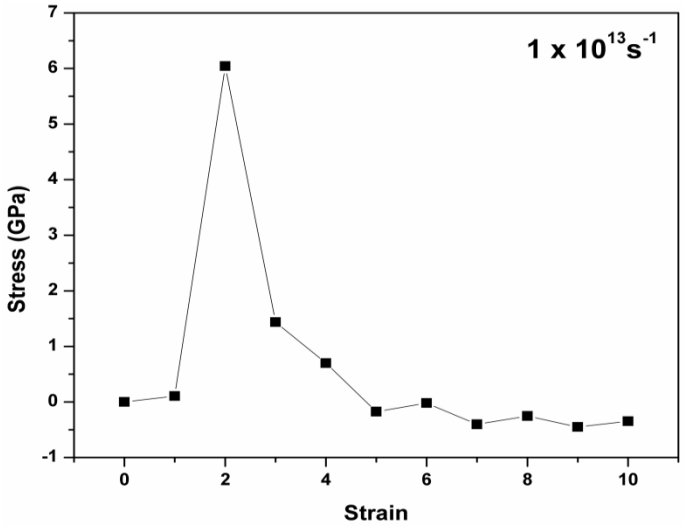

Fig. 4.20: Engineering stress-engineering strain plot for size 100Å x 50Å x 100Å at strain rate 10^{13} s^{-1}.

Comparison of the stress-strain curves at different strain rates for the simulation box size of 100Å × 50Å × 100Å (43904 atoms):

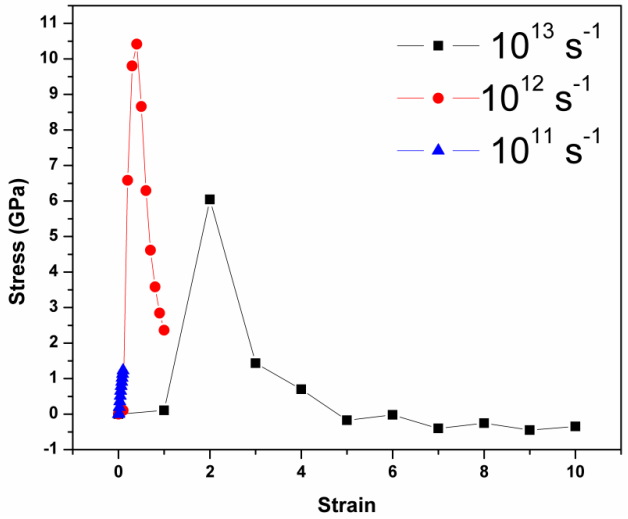

Fig. 4.21: Comparison of engineering stress-engineering strain plots at different strain rates for $Cu_{50}Zr_{50}$ amorphous alloy model of size 100Å × 50Å × 100Å.

From the Fig. 4.21, we can conclude that increase in strain rate increases the flow stress. However at strain rate of 10^{13} s^{-1} due to the formation of voids at the early stage of deformation there is sharp decrease in stress compared to the other strain rates.

4.5 Contour plots for size x=50Å y=30Å z=20Å at strain rate 10^{11} s^{-1}:

Contour plot is the two dimensional representation of three dimensional data. A contour plot is a graphical technique to represent a 3-dimensional surface by plotting constant z slices called contours. Lines are drawn for a given value of z for connecting the (x, y) coordinates where that z value occurs. This contour plot is an alternative to a 3-D surface plot.

Metallic glasses having disordered structure and absence of crystallographic planes necessitates for studying the stress distribution in the present model metallic glass. The following figures show the contour plots of shear stress distribution on the group of atoms.

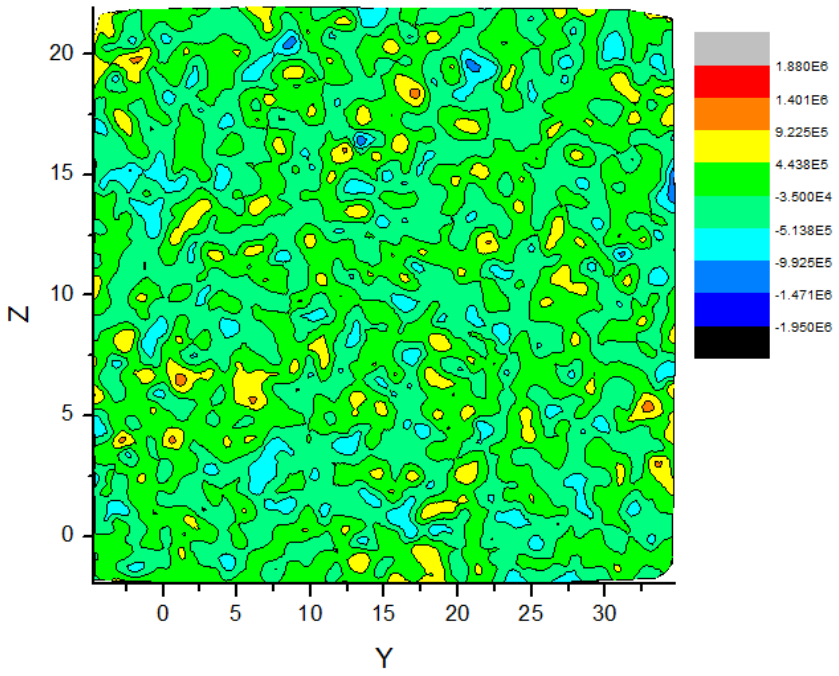

Fig. 4.22: Contour plot for Shear stress τ_{xy} on y-z plane

In the Fig. 4.22, shear stress τ_{xy} has been plotted against Y and Z coordinates. Regions of different colors correspond to different shear stress values as indicated in the right side of the plot. Since different regions corresponds to different shear stress values, so different atoms in the above plane are experiencing different values of shear stress. For a particular region of the plane the prominent color in that region gives the most probable shear stress value (the stress experienced by the maximum no of atoms in that region).

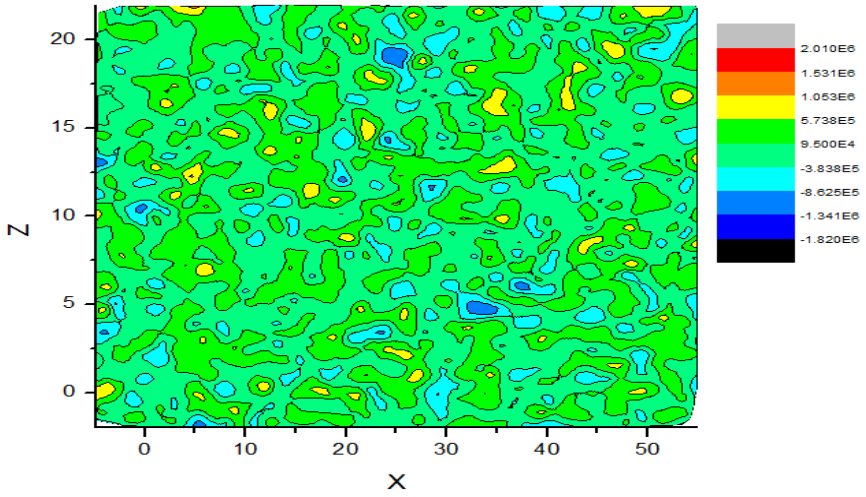

Fig. 4.23 Contour plot for Shear stress τ_{yz} on x-z plane

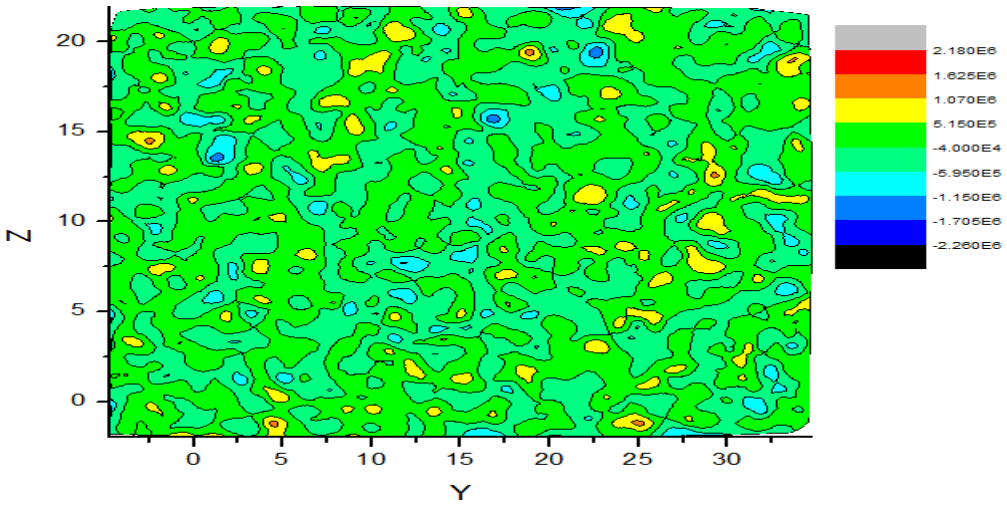

Fig. 4.24 Contour plot for Shear stress τ_{xz} on y-z plane

For the Fig. 4.23 & Fig 4.24, similar interpretation can be done like Fig. 4.22.

4.6 Fracture Behavior:

Simulation studies have been also done to study the initiation of fracture during tensile deformation at different strain rates varying from 10^{11} s^{-1} - 10^{13} s^{-1}. In this study simulation was done in a similar way as described in section 4.4 only the difference was that deformation was carried out for a longer period of time to see fracture at different strain rates keeping the total simulation time fixed. So in.file for fracture is same as that given in section 4.4 with only change in strain rate concerned and change in no of iterations in the last command of in.file ,which is in this case 3500 instead of 1000. The VMD images and subsequent stress-strain plots are given below:

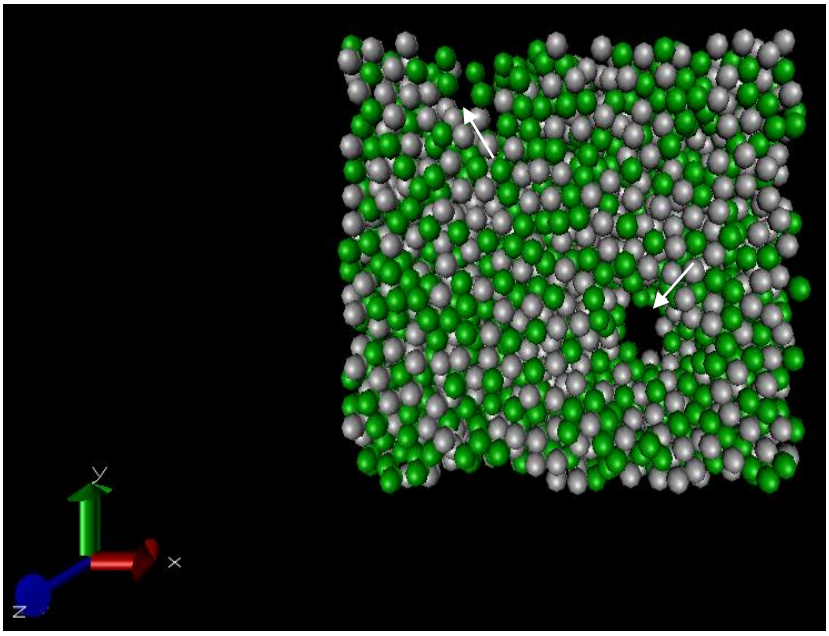

Fig. 4.25: VMD snap shot of $Cu_{50}Zr_{50}$ model glass of size 50Å × 30Å × 20Å showing voids (indicated by arrow) which are formed after 3.5ps during tensile deformation at strain rate of 10^{11} s^{-1}.

Table 4.6: Stress-strain data for size 50Å × 30Å × 20Å at strain rate of 10^{11} s^{-1} up to 3.5ps of simulation time.

Stress (GPa)	Strain
0.12535	0.01
0.80285	0.02
1.5232	0.03
2.27845	0.04
3.02736	0.05
3.7128	0.06
4.3792	0.07
4.88059	0.08
5.59072	0.09
6.0928	0.1
6.4736	0.11
6.92758	0.12
7.36213	0.13
7.67404	0.14
7.99591	0.15
8.15547	0.16
8.44107	0.17
8.69493	0.18
8.79013	0.19
8.88533	0.2
9.044	0.21
9.10747	0.22
9.1392	0.23
9.15583	0.24
9.07573	0.25
8.98053	0.26
8.66533	0.27
8.39654	0.28
7.90677	0.29
7.55253	0.3
7.22311	0.31
6.69573	0.32
6.3784	0.33
5.96587	0.34
5.42802	0.35

Based on the data given in Table 4.6, the stress-strain plot obtained has been shown below:

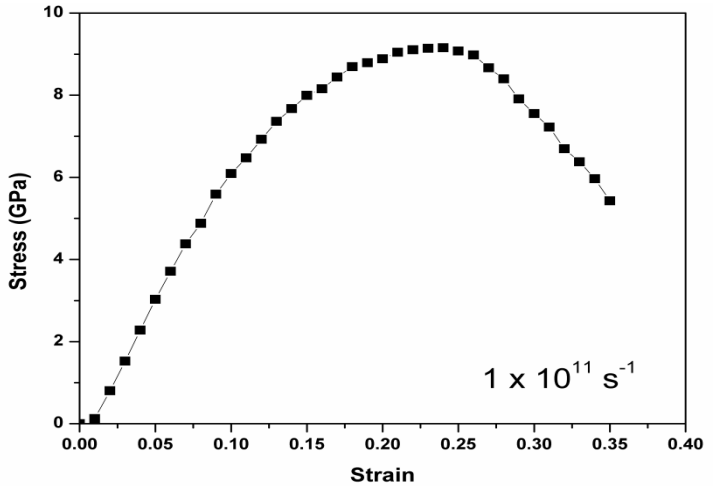

Fig. 4.26 Engineering stress-engineering strain plot for size 50Å × 30Å × 20Å at strain rate of 10^{11} s^{-1} up to 3.5 ps of simulation time.

The above stress-strain plot shows the sample fractured by formation of voids. The sample exhibits UTS of 9 GPa and fracture stress of 5 GPa. The decrease in stress is due to formation of voids at different locations of the sample.

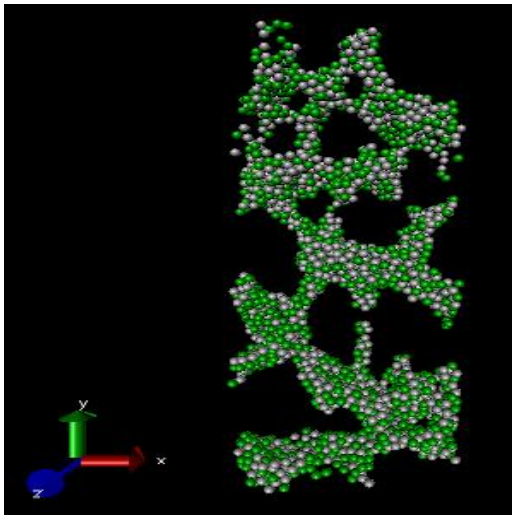

Fig. 4.27: VMD snap shot of $Cu_{50}Zr_{50}$ model glass of size 50Å × 30Å × 20Å showing voids which are formed after 3.5ps during tensile deformation at strain rate of 10^{12} s^{-1}.

Fig. 4.27 shows the sample of size (50Å × 30Å × 20Å) which was subjected to a uniaxial tensile deformation at a higher strain rate of 10^{12} s^{-1} and after the same time interval of 3.5 ps, the sample fails by formation of voids at several locations reaching its final separation undergoing a series of localized fractures .

Table 4.7 Stress-strain data for size 50Å × 30Å × 20Å at strain rate 10^{12} s^{-1} after 3.5ps of simulation.

Stress (GPa)	Strain
0.12535	0.1
6.2474	0.2
10.12293	0.3
11.49346	0.4
9.996	0.5
7.42658	0.6
5.23207	0.7
3.90098	0.8
2.9896	0.9
2.50522	1
2.13423	1.1
1.99212	1.2
1.787	1.3
1.70532	1.4
1.47553	1.5
1.22712	1.6
1.27251	1.7
1.06476	1.8
1.03451	1.9
1.00912	2
0.99039	2.1
0.96404	2.2
0.99325	2.3
0.80603	2.4
0.78699	2.5
0.73365	2.6
0.77356	2.7
0.68288	2.8
0.70131	2.9
0.5712	3
0.50762	3.1
0.63531	3.2
0.66112	3.3
0.55151	3.4
0.65834	3.5

Based on the data given in Table 4.7, the stress-strain plot obtained has been shown below:

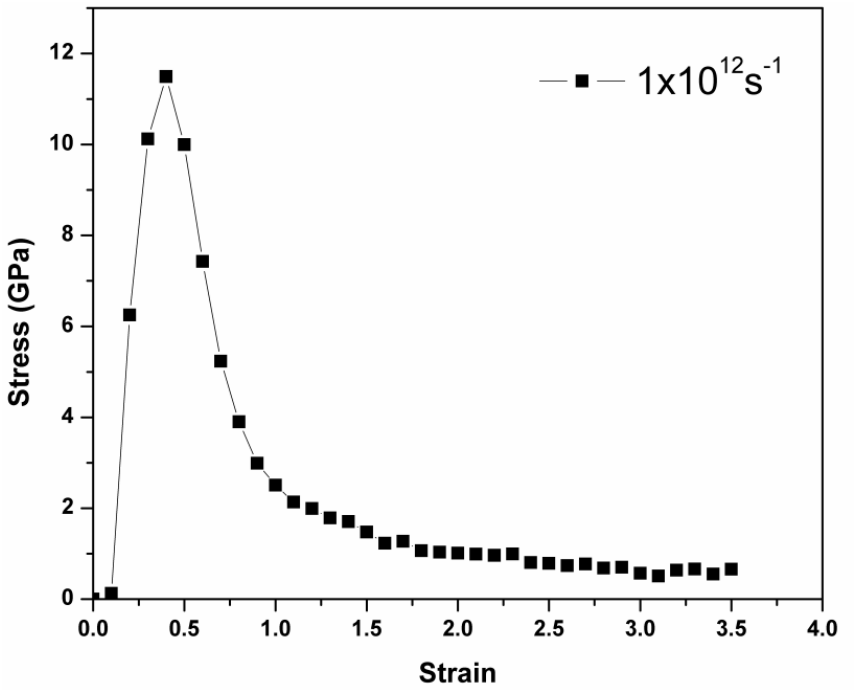

Fig. 4.28 Engineering stress-engineering strain plot for size 50Å × 30Å × 20Å at strain rate 10^{12} s^{-1}. The drop in the stress indicates initiation of void.

It can be seen from Fig. 4.26 and Fig. 4.28 that increase in strain rate decreases the time to rupture.

5. Conclusions

Form the MD simulations studies on the effect of size and strain rate on the deformation behavior of $Cu_{50}Zr_{50}$ metallic glass we conclude that

1. There was no significant change in the nature of the stress-strain curves with increasing the sample height (number of atoms).
2. Flow stress decreased with increase in cross-section size of the sample deformed at strain rate of 1×10^{11} s^{-1}.
3. With increasing strain rate from 1×10^{11} s^{-1} to 1×10^{12} s^{-1} flow stress increased while that at strain rate of 1×10^{13} s^{-1} there was significant drop in the stress due to nucleation of voids and leading to early fracture.
4. With increase in strain rate the time to rupture decreased.
5. Contour plots suggest that the stress distribution was not uniform throughout the sample.

FUTURE WORK:

a. Temperature effect on the deformation behavior of $Cu_{50}Zr_{50}$ metallic glass.
b. Shape effect on the deformation behavior of $Cu_{50}Zr_{50}$ metallic glass.
c. Study on the effect of short range orders (SROs) and Medium range orders (MRO) in $Cu_{50}Zr_{50}$ metallic glass.
d. Study of effect of different quenching rates on deformation behavior of $Cu_{50}Zr_{50}$ metallic glass.

References:

[1] www.wikipedia.com

[2] Klement W, Willens R H, Duwez P, (1960), Non-crystalline Structure in Solidified Gold-Silicon Alloys, *Nature, Vol* 187**,** pp. 869–870.

[3] Libermann H and Graham C, (1976), Production Of Amorphous Alloy Ribbons And Effects Of Apparatus Parameters On Ribbon Dimensions, *IEEE Transactions on Magnetics Vol* 12**,** p. 921.

[4] Inoue, A., and Takeuchi A. (2004), Recent progress in bulk glassy, nanoquasi and nanocrystalline alloys, Materials Science and Engineering, Vol. A 375, pp. 16-30.

[5]Chen H S, (1980), Glassy metals, Vol 43, pp. 354-432. [4] Spaepen Frans, (1976), A microscopic mechanism for steady state inhomogeneous flow in metallic glasses, Acta Metallurgica, Vol 25, pp. 407-415.

[6] Spaepen Frans, (1976),A microscopic mechanism for steady state inhomogeneous flow in metallic glasses, Acta Metallurgica, Vol 25,pp. 407-415.

[7] Schuh Christopher A, Lund Alan C, (2003), Atomistic basis for the plastic yield criterion of metallic glass, nature materials, Vol 2, pp. 449-452

[8] Shin Takeuchi, Keiichi Edagawa (2011), Atomistic simulation and modeling of localized shear deformation in metallic glasses, Vol,56, PP. 785-816.

[9] Malandro D L, Lacks D J, (1999), size effect of shear deformation in a monatomic model metallic glass, Vol 110, p. 4593.

[10] Ogata Shigenobu, Shimizu Futoshi, Li u,WakedaMasato,ShibutaniYoji,(2006),Atomistic simulation of shear localization in Cu–Zr bulk metallic glass, Intermetallics., Vol 14,pp. 1033-1037.

[11] Sergueeva A.V, Mara N.A, Kuntz J.D, Branagan D.J, Mukherjee A.K ,(2004), Shear band formation and ductility of metallic glasses,Maret. Sci. Eng.,Vol A 383, pp. 219-223.

[12] Duhamel C,Das j,Pauly S, Eckert J,(2008), Effect of Titanium on Microstructure and Mechanical Properties of $Cu_{50}Zr_{50-x}Ti_x$ ($2.5 \leq x \leq 7.5$) Glass Matrix Composites Meta. And Mater.Transactions,Vol 39A,pp. 1868-1873.

[13] Zhang Z.F, Eckert J, Schultz L,(2003), Difference in compressive and tensile fracture mechanisms of $Zr_{59}Cu_{20}Al_{10}Ni_8Ti_3$ bulk metallic glass,Acta Materialia,Vol 51,pp. 1167–1179.

[14] www.lammps.sandia.gov